2006

Tyrosinase-like activity of several Alzheimer's disease related and model peptides and their inhibition by natural antioxidants

Kashmir Singh Juneja
University of South Florida

Tyrosinase-like Activity of Several Alzheimer's Disease Related and Model Peptides and their Inhibition by Natural Antioxidants

by

Kashmir Singh Juneja

A thesis submitted in partial fulfillment
of the requirements for the degree of
Master of Science
Department of Chemistry
College of Arts and Sciences
University of South Florida

Major Professor: Li-June Ming, Ph.D.
Steven Grossman, Ph.D.
Kirpal Bisht, Ph.D.

Date of Approval
November 13, 2006

Keywords: Alzheimer's, Amyloid, Flavonoids, Tyrosinase, Metzincins

Dedication

This thesis is dedicated to the near 16 million people with Alzheimer's disease. It is my hope that this work contributes to the understanding and ultimately treatment for this horrendous disease.

Acknowledgments

My undergraduate mentor Vasiliki (Vaso) Lykourinou. I consider this woman a saint for maintaining sanity after being in the lab with so many children. Her patience and commitment is something that I am very envious and thankful for.

William Tay, with the exception of the consistent threats on my life, inability to make a lay-up, and horrible sense of direction, Tay has become a good friend who has provided nothing but positive support.

Giordano da Silva, a boy amongst men, who trained under the finest Mongolian monk, has passed much of his knowledge on to me. Over the past five years he has constantly reminded me people don't hate me for the color of my skin, it's because of my personality.

Erin Wu, for showing me the possibility to study abroad without ever learning the native language. I thank you for making me realize Labor Day falls on the day(s) I want it to.

Dr. Ming, without meeting him my daily diet would still consist of subway, hot dogs, and microwave meals. With the exception of making me work with Gio, I appreciate Dr. Ming for everything he has done for me, as it has helped me mature both mentally and culturally.

My better half, Joumana Aram. For her devotion, tolerance, and support.

And of course my parents, brother, and grandfather, for their support, without them, I would have never made it this far.

Table of Contents

List of Tables

List of Figures

List of Abbreviations

$A\beta^{16}$	Beta-amyloid – 16 amino acid
$A\beta^{20}$	Beta-amyloid – 20 amino acid
AsA	Ascorbic acid
BP10	Blastula Protease 10
EC	Epicatechin
EDTA	Ethylenediamine tetraacetic acid
EGC	Epigallocatechin
EGCG	Epigallocatechin gallate
GTC	Green Tea Catechin
HEPES	N-[2-Hydroxyethyl]piperazine-N'-[2-ethanesulfonic acid]
MBTH	3-methyl-2-benzothiazolinone hydrazone hydrochloride monohydrate
ROS	Reactive oxygen species

Tyrosinase-like Activity of Several Alzheimer's Disease Related and Model Peptides and their Inhibition by Natural Antioxidants

Kashmir Singh Juneja

ABSTRACT

Neurodegenerative diseases are associated with loss of neurons ultimately leading to a decline in brain function. Alzheimer's disease (AD) is considered one of the most common neurodegenerative disorders that affects 16 million people worldwide. The cause of the disease remains unknown, although significant evidence proposes the amyloid β-peptide (Aβ) as a potential culprit. The binding of Cu^{2+} by the soluble fragments of Aβ have shown to form Type-3 copper centers and catalyze the oxidation of catechol-containing neurotransmitters. Furthermore, the use of flavonoids as antioxidants to slow or inhibit the neurotransmitter oxidation has suggested further health benefits with their consumption. A structure-function correlation is also made between the flavonoids and their reactively with Cu^{2+}-Aβ. Mechanistic insight into the binding of catechol and dioxygen within the tyrosinase-like mechanism are made using a metallopeptide modeling the active site of the metzinicins.

Chapter One

Introduction

Enzymes

Enzymes are essential proteins that have the ability to regulate and govern numerous reactions required for life. They serve as biological catalysts, reducing the energy barrier in a reaction. The catalytic proficiency is further enhanced by an enzyme's ability to be substrate specific. In general, enzymes can be categorized on the basis of the type of reaction in which they perform. Examples include oxidoreducatses, hydrolases, and transferases.

The catalysts that fall under the oxidoreducatase category are involved in redox reactions. These redox reactions involve the transfer of electron(s) from one species to another.[1] Redox reactions are involved extensively in industrial application, humus degradation, and are essential for life on this planet. Biological systems use these oxidoreductases in anabolism, catabolism, protective, and energy sublimentive functions.[2] Being that the inside of the cell is under reductive conditions, these enzymes are used to regulate and specify when and where a redox reaction takes place.

In biological systems, constitutes formed are sometimes the result of several enzymes. Whether the product is modified or the enzyme is regulated, it is usually a cascade of reactions that is involved in synthesizing the necessary biological components. Hydrolases are another class of enzymes that activate a water molecule to serve as a nucleophile in a substrate-specific bond cleavage.[2] These hydrolytic enzymes are further classified on the basis of their substrate specificity. An example is endopeptidases which

cleave peptide bonds within a peptide or protein at specific locations other then C and N-terminal domains. The structure of the protein, specifically the active site, controls the specificity of the enzyme. In many enzymes, metals ions can be found within the active site to assist in catalysis.

Transition metals are excellent Lewis acids that have the ability to carry a charge and still contain a high electron affinity.[3] In an effort to continue catalysis, metal ion(s) undergo a degree of mobility by making slight changes in its coordination during a reaction. The differences in metal ions allow each to prefer particular geometries and types of chemistry.[3] Table (1-1) summarizes information about several well-known metalloenzymes.

Table 1-1. Information on some metalloenzymes.

Metalloenzyme	Metal Ion(s)	Occurrence	Function
Reverse Transcriptase[3]	Zn	Human immunodeficiency virus (HIV)	Transcribes ssRNA into dsDNA
Tyrosinase[3]	2 Cu	Plants and Animals	Hydroxylation and oxidation of phenol
Lipoxygenase[3]	Fe	Animals	Catalyse the dioxygenation of polyunsaturated fatty acids
Methionine aminopeptidase[3]	2 Co	Bacteria to Animals	Removal of N-terminal methionine
Urease[3]	2 Ni	Jack Bean and bacteria	Hydrolysis of urea to ammonia
Mn-catalase[3]	2 Mn	Prokaryote	Decomposition of $2\ H_2O_2 \rightarrow 2\ H_2O + O_2$
Bromoperoxidase[3]	V	Some brown & red marine algae	Defensive Mechanism
Chromodulin[4]	Cr	Human	Unknown, possible insulin signaling
DMSO reductase[3]	Mo	Bacteria	Dimethyl sulfoxide to dimethyl sulfide
Acetylene hydratase[3]	W	Pelobacter acetylenicus	Hydration of acetylene to acetaldehyde

Metzincins

The function of a metalloenzyme can be related to the transition metal ion(s) within its active site. Of the transition metals, zinc is one of the most readily available to biological systems, ranging from 10^{-11} to 10^{-3} M in various portions of a cell.[3] Zn(II) ion has the electronic configuration of [Ne] $3d^{10}$, lacking both spectroscopic and magnetic properties. Like many of the first row transition metals, zinc is often found in divalent state (Zn^{2+}) because of the loss of the $4s^2$ electrons. When considering divalent cations, Zn^{2+} is an excellent Lewis acid, second only to Cu^{2+}.[3] The unique properties of Zn^{2+} also include extremely flexible coordination geometry extending, from 4 to 6 coordination. The most common ligands for Zn^{2+} are thiolate, imidazole, water, and carboxylate. The Zn^{2+} found in metalloenzymes can serve a structural role or be involved in the reaction. For example, the Zn^{2+} in Cu,Zn-superoxide dismutase serves a structural role that stabilizes the protein.[3] In other cases Zn^{2+} is involved in reactions, where in the metalloenzymes most always perform hydrolysis. The classification of these hydrolytically active Zn^{2+} enzymes is based on the ligands coordinated to the metal ion and the substrate specificity.

For the past two decades, several large groups of Zn^{2+}-containing enzymes have received much attention because of similarities in their structure and distinctive location. The following groups have been classified as zinc endopeptidases: astacins, adamalysins, serralysins, matrixins.[5] These endopeptidases contain a common α-helical Zn^{2+} binding motif (HEXXHxxGxxH) and a distant methionine turn (Figure 1.1). It is because of these similarities that all of these families have been grouped into one super family called the metzincins.[5] Despite their common structure, the metzincins have been found in

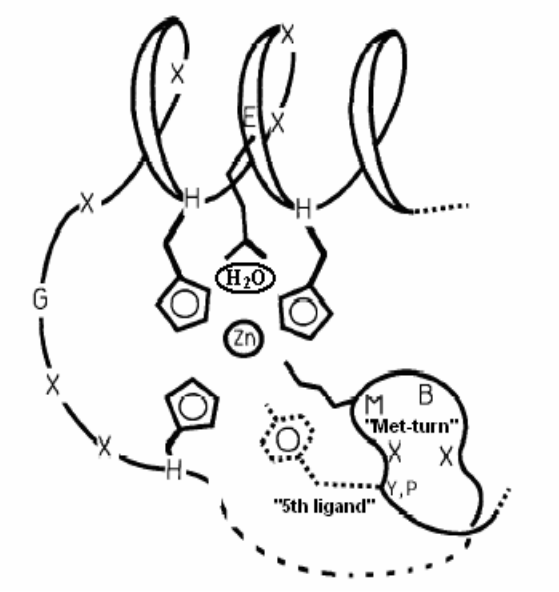

Figure 1-1: Diagram of the zinc environment in the metzincins.[5]

numerous locations including caryfish digesitive fluid, sea urchin embryos, and snake vemon.[5,6] In the metzincins, the metal is coordinated by 3 His side chains and a water molecule which is H-bonded to the Glu in the motif.[5] Most recent evidence reveals a distant Tyr after the Met-turn in astacin, which stabilizes the enzyme-substrate complex through H-bonding and relieves steric hindrance.[7] In addition, several studies have shown accelerated hydrolytic activity upon substitution of the native Zn^{2+} with Cu^{2+} or Co^{2+}.[7,8]

It is evident through the properties and abundance of Zn^{2+} that this unique transition metal is one of the most important in biological systems. The flexibility and ligand exchange rate haveforced nature to develop a dynamic scheme of delivery of this precious metal.[3] Metal substitution experiments have postulated nature's use of Zn^{2+} instead of another transition metal because of its inertness in redox chemistry.

Copper-Containing Enzymes

Copper-associated chemistry is very rich in nature. Exceeding all other transition metals, Cu^{2+} is a very effective divalent ion for binding organic ligand molecules.[3] The high electron affinity makes it a valuable asset in biological redox chemistry. Several Cu-containing enzymes can bind and activate small molecules such as O_2.[3] It is the affinity for these molecules and large redox potential that has forced nature to developed specialized transport systems to maintain homeostasis and limit free Cu^{2+} to 10^{-18} M in the human body.[9]

To replenish the body, it is recommended to consume 0.9 mg of copper per day.[9] Copper is absorbed mainly in the small intestine and transported to the liver. Here, transporters and chaperons deliver the metal to various locations in the body. One of the main transports is human copper transport protein (hCtr1).[9] Together with the influx of potassium (K^+), copper is taken up and delivered to several chaperons or storage structures such as the metallothionein pool.[3] The chaperons in turn supply Cu to proteins like superoxide dismutatse, amyloid precursor protein (APP) dopamine β-hydroxylase, and tyrosinase. The role of many Cu enzymes is O_2 activation followed by oxidation of a substrate.[10] The mechanistic differences within Cu-proteins are due to the protein structure, the number of Cu ions, and the coordination chemistry.

The copper within proteins is usually limited to one of three types of coordination. Each copper protein can be categorized as Types I-III. Type I copper proteins are well-known for their intense blue color and consist of blue Cu-proteins and blue Cu-oxidases.[11] The blue Cu-proteins contain one copper ion coordinated by two histidines, one cystein, and one loosely coordinated methionine in a trigonal or trigonal bipyrimadal

conformation.[11] An example of a Type I copper protein is the electron transfer protein plastocyanin in photosynthesis. The active site of Type II copper protein is usually coordinated by both nitrogen and oxygen-containing ligands in a tetragonally distorted configuration.[11] A well-known Type II copper enzyme is the radical scavenging Cu/Zn-superoxide dismutase. The third group of copper proteins are the EPR silent Type III copper proteins. These copper proteins contain two copper ions as a dinuclear center coordinated by six histidine residues.[11] One of the best known examples is tyrosinase.

To date, tyrosinase is considered one of the most well studied multicopper oxygenases. Found widely in living systems, tyrosinase is responsible for the preliminary steps in the synthesis of melanin.[12] Like all Type III copper proteins, tyrosinase utilizes its dinuclear center to bind dioxygen. Following the subsequent activation of O_2, it hydroxylates and oxidizes the phenolic substrate to yield the ortho-quinone product (Figure 1-2).[12] The rates for the oxidation (10^7 s^{-1}) is ten thousand times that of the hydroxylation (10^3 s^{-1}).[11] To determine the mechanism and its intermediates, nitrogen-based model systems have been used extensively.[13]

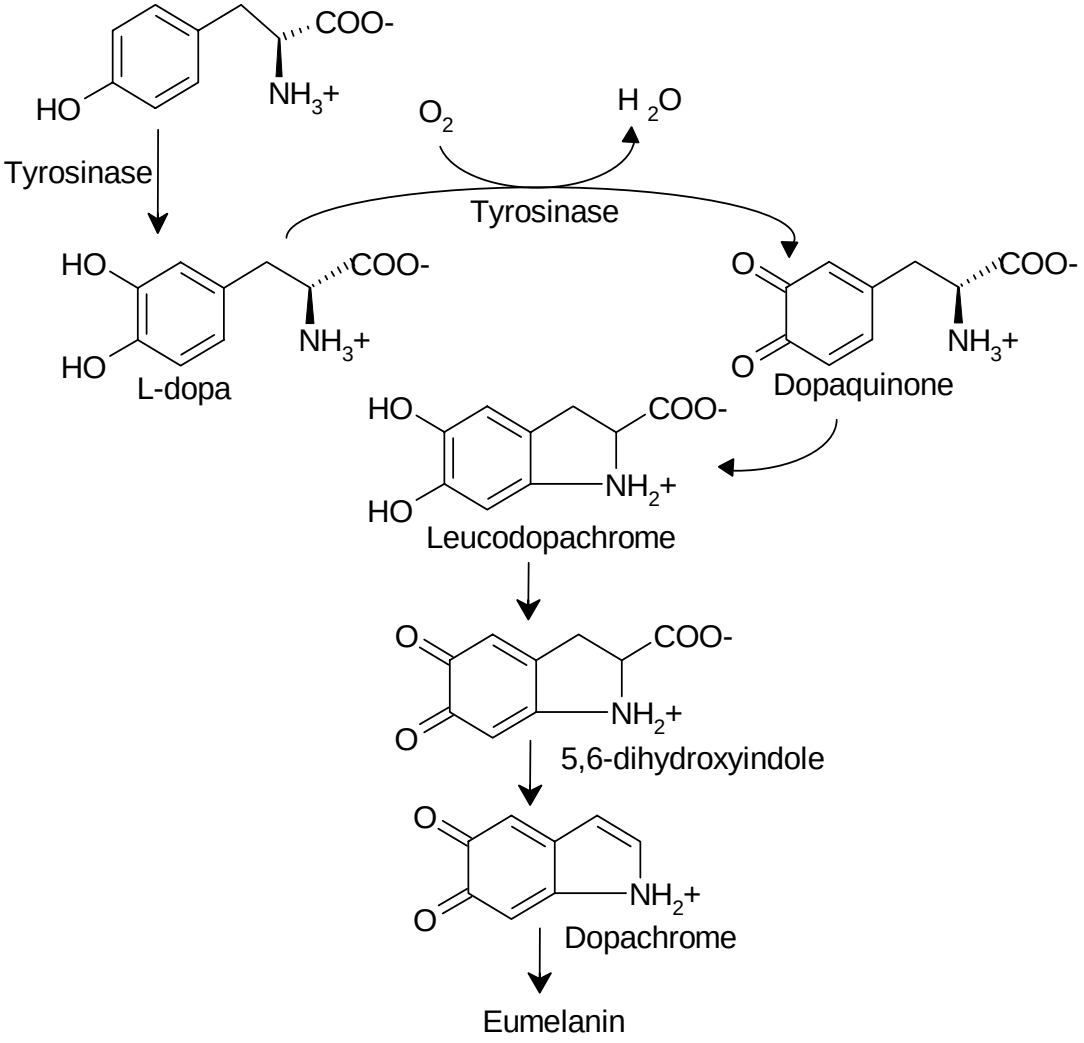

Figure 1-2: Scheme depicting tyrosinase activity in the production of melanin.[12]

The reaction at the dinuclear center of tyrosinase begins with the binding of dioxygen, converting the deoxy into the oxy form of the dinuclear center. Monophenol then binds to one of the copper centers, allowing for it to be oriented for ortho hydroxylation. The hydroxylation is believed to go through one of three intermediates

(Figure 1-3).[11] One intermediate involved the oxygen bridge cleavage prior to attack, resulting in the formation of a binuclear Cu^{3+}.[11] The second is the breakage of the oxygen bridge with the attack.[11] And lastly, is a possible aryl peroxide intermediate.[11] The resulting diphenol is bound to the "met-D" center (Figure 1-4), allowing for a two-electron oxidation to form the o-quinone. In addition to the monophenolase activity, tyrosinase can oxidize catechol (diphenols) directly. Both the met and oxy forms of the dinuclear center can bind and promote the oxidation of catechol. The reaction continues in this cycle until the substrate has been depleted or the enzyme is inhibited.

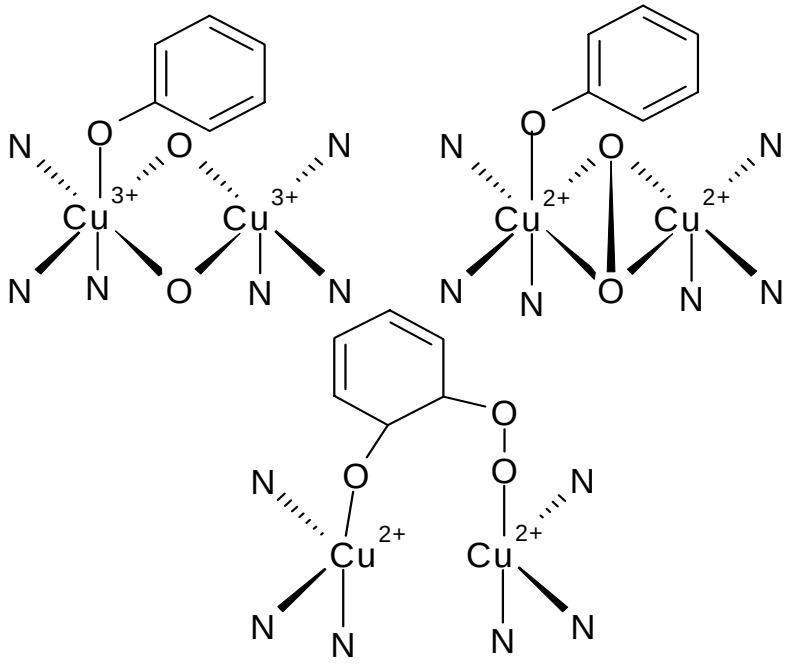

Figure 1-3: Three proposed intermediates for the hydroxylation of phenol by tyrosinase.[11]

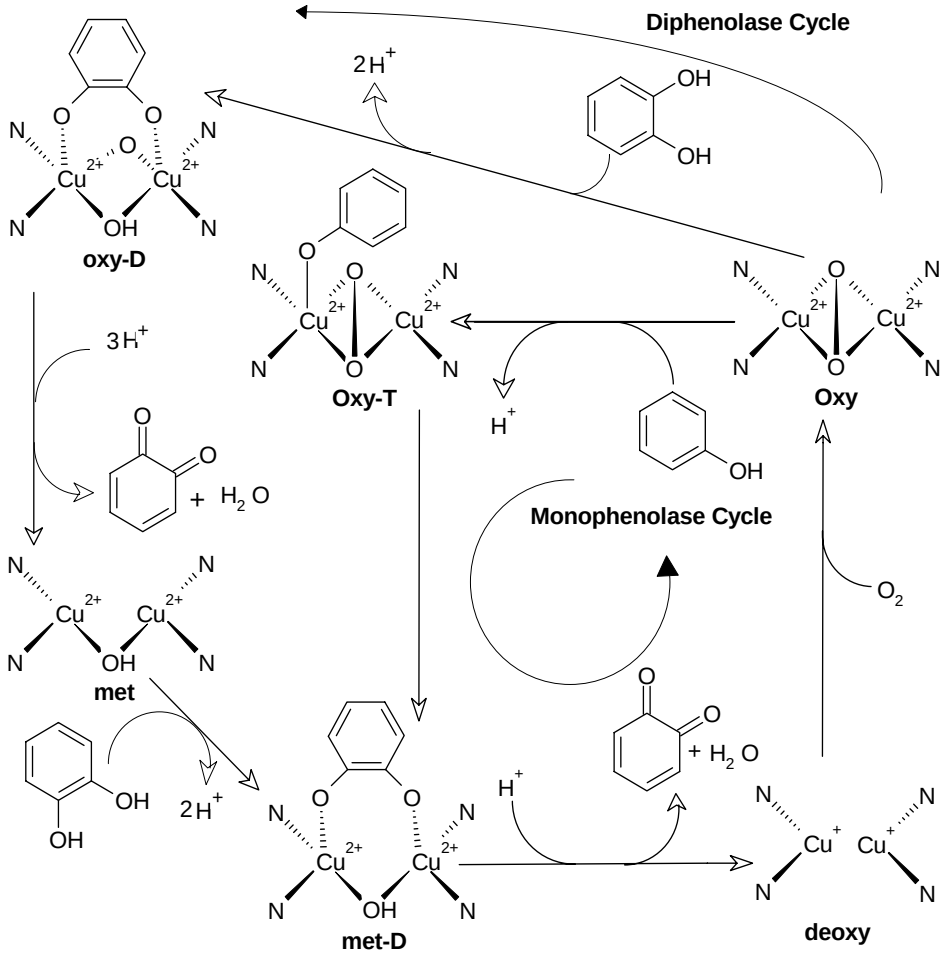

Figure 1-4: Proposed mechanism for tyrosinase.[11]

The intermediates and mechanism for tyrosinase were solved using various synthetic metal complexes as model systems. The structure of these complexes varies but generally contain N-based functional groups such as amine, pyridyl, pyrazolyl, and imidazole.[14] Through the use of numerous spectroscopic techniques and low-temperature experiments, a number of plausible Cu:O_2 intermediates have been found.[10] However,

these model systems have been shown to contain reduced tyrosinase activity. The modeling of active sites for activity and binding is an ever growing trend that extends to far beyond just Type III copper proteins.[15]

Amyloid-β and Alzheimer's Disease

Through advances in modern medicine, the duration of life has been extended by eliminating or postponing various human diseases. Unfortunately, with the average life span almost doubling from the 19th century there has been a significant increase in aging-related illnesses.[16] Neurological disorders such as Alzheimer's, Parkinson's, and Huntington's disease, have caused increased concern for the ever-growing number of victims. The most common neurodegenerative disease is Alzheimer's (AD), affecting near 4.5 million Americans.[17] With only 10% of the cases being familial AD, the majority of the occurrences are sporadic and currently unpredictable.[17] In general, a neurodegenerative disease is associated with the accumulation of misfolded or fragmented protein that affects normal neuronal function.[9]

AD is a progressive neurodegenerative disease that causes memory and motor skill loss. There are three hallmarks associated with AD which are believed to be responsible for the loss of neuronal function, located primarily in the hippocampus and cortex: (a) accumulation of neurofibrillary tangles composed of the hyperphosporylated microtububle-associated tau protein (p-tau), (b) insoluble plaques formed from the amyloid-β peptides (Aβ), and (c) ramped loss of neurons.[9,18] Even though the exact cause of AD is still unknown, many have hypothesized an amyloid cascade leading to all three of the hallmarks.

Even with slight variations, it has been agreed upon that the abnormal processing of the transmembrane amyloid precursor protein (APP) causes an increase in the production of Aβ.[11,17] This overproduction is believed to affect synapses, causing altered ionic and enzymatic homeostasis resulting in tangles, plaques, and ultimately cell death.[9] The order and location of cleavage by three secreatases (α, β, γ) determine whether the product will be considered amyloidogenic or nonamyloidogenic.[9] The nonamyloidogenic pathway begins with the α-secreatase cleavage followed by a γ-secreatase forming a shorter more soluble fragement of Aβ.[9] The amyloidogenic pathway is initiated by β-secreatase followed again by γ-secreatase.[9] The fragments of APP following cleavage range from 16-42 amino acids in length (Figure 1-5), with the insoluble $A\beta^{40}$ and $A\beta^{42}$ believed to have the largest effect on neuronal cell loss.[9,18]

$DAEFR^{5}HDSGY^{10}EVHHQ^{15}KLVFF^{20}AEDVG^{25}SNKGA^{30}IIGLM^{35}VGGVV^{40}IA^{42}$

Figure 1-5: Amino acid sequence of Amyloid-β peptides (Aβ).

In addition to the accumulation of protein fragments, postmortem studies have reported millimolar amounts of Zn^{2+}, Cu^{2+}, and Fe^{3+} within the amlyoid plaques.[17] The findings of redox-active metals have fueled the hypothesis of reactive oxygen species (ROS) as a major contributor to the degradation of brain function in AD. The ROS species normally generated by the body are used for degradation and defense purposes.[2] The body regulates ROS by both SOD and catalase. The hypothesis that ROS is part of AD is well justified as non-regulated accumulation of redox active metal has led to other

illnesses such as Wilson's Disease (WD).[9] The metal-centered generation of ROS is believed to be consistent with the Fenton and Haber-Weiss reactions shown below.[9]

$$O_2^- + H_2O_2 \rightarrow OH^- OH^{\bullet} + O_2 \quad \text{(Haber-Weiss reaction)}$$

$$M^{n+} + H_2O_2 \rightarrow OH^- + OH^{\cdot} + M^{(n+1)+} \quad \text{(Fenton reaction)}$$

Studies have shown that APP is an active participant in copper homeostasis, with significant loss of this protein showing elevated levels of free Cu^{2+}.[9] Not surprising is that Aβ has also shown to chelate metal with a high affinity.[19] Through the use of NMR, the binding site for the metal has shown to be three His within the first 14 amino acids.[20] Additional studies have shown the possible dimerization and coagulation of Aβ to begin at amino acid 17-20.[21] Although much emphasis has been put on $A\beta^{40,42}$, numerous structure studies are focused on all of the Aβ and possible ways to inhibit its formation.

To date, treatments for AD include metal chelators and acetylcholine esterase inhibitors. Unfortunately there are many side effects associated with the metal chelators, specifically due to the chelation of "needed" metal ions. The binding of redox-active metals to solvent-exposed peptide domains has raised the issue of possible ROS generation in AD. This emphasizes the development of bioavailabile metal chelators or the use of antioxidants to scavenge ROS.

Flavonoids

In ancient China, there had been evidence of the use of antioxidants as a remedy to cure human illness. Of these antioxidants, a group of phenolic plant constituents encompass a major portion of those consumed around the world for their potential benefits. To date, there are over 6000 of these compounds known as flavonoids.[22]

Several clinical studies have been done concerning the possible protection against cancer, cardiovascular, and neurodegenerative diseases.[23,24] They have been further used for their potential anti-fungal, anti-microbial, and anti-radical properties.[22]

Flavonoids have gained much attention over the years because of their potent antioxidant properties and bioavailability. The structural differences of the flavonoids, although subtle, have shown to remarkable change their bioactivity.[25] It is these differences that allow the flavonoids to be divided into subcategories. The general structure consists of two benzene rings (A and B) linked though a tetrahydropyran or α-pyrone ring (C).[22] Flavones (e.g. apigenin) contain a double bond at the 2-3 position, while flavanones (e.g. narigenin) are staturated at this position. A double bond at the 2-3 position and a hydroxyl, methoxy, or sugar at the 3 position represents the flavonol category (e.g. quercetin, fisetin). Dihydroflavonols contain a hydroxyl group at the 3 position and is absent of the 2-3 double bond. The catechins lack the ketone functionality in the C ring and contains hydroxyl groups at 3, 3', and 4' positions. Many other classifications exist for flavonoids that contain further unsatutartion, hydroxylation, epoxidation, and sugar modification. Table 1-2 describes the structure of several well studied flavonoids.

The quantity of each group of flavonoids depends on the kind of plant, climate, and location the plant is found. For example, several categories are found in higher amount in citrus, while others are found in green-leaf vegetables.[22] Although there is an abundance of flavonoids within the diet, their protective properties are only good as they are absorbed. Several flavonoids have better absorptive properties then others. It has

Table 1-2: The classification and structure of several well studied flavonoids.

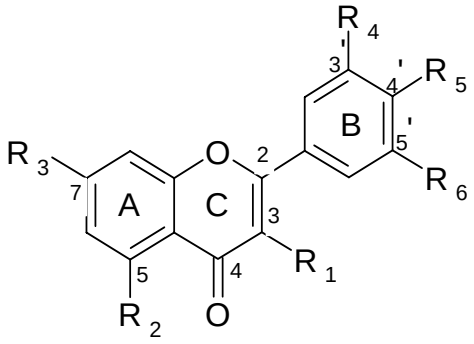

Flavonoids	Classification	R1	R2	R3	R4	R5	R6	2-3 Alkene	4 Ketone
(-)-Epicatechin	Flavan-3-ol	H	OH	OH	OH	OH	H	-	-
(-)-Epigallocatechin Gallate	Flavan-3-ol	Gallate	OH	OH	OH	OH	OH	-	-
Fisetin	Flavonol	OH	H	OH	OH	OH	H	+	+
Quercetin	Flavonol	OH	OH	OH	OH	OH	H	+	+
Taxifolin	Dihydroflavonol	OH	OH	OH	OH	OH	H	-	+
Apigenin	Flavone	H	OH	OH	H	OH	H	+	+
Narigenin	Flavone	H	OH	OH	H	OH	H	-	+
Hesperetin	Flavanone	H	OH	OH	OH	OCH_3	H	-	+
Rutin	Flavonol glycoside	Rutinose	OH	OH	OH	OH	H	+	+

been shown that lactase and β-glycosidase can cleave the glucoside portion off the sugar derivatives of flavonoids.[22] It is the effects following absorption that has increased the interest in the natural polyphenols.

With numerous illnesses and disease being associated with ROS, the antioxidant and antiradical properties of flavonoids have become the center of attention. For a compound to be considered a strong antioxidant it must inhibit oxidation reactions and/or the production of radicals at a low concentration compared to the oxidizable substrate.

Furthermore, the radicals formed by flavonoids must be stable enough not to continue in as a chain propagating radical. These properties associated with flavonoids have been used in conjunction with other molecules to further stabilize or complement the flavonoids bioactivity.[26]

Green Tea

Believed to have originated some 3000 years ago in ancient China, tea is now one of the most consumed beverages in the world.[27] The leaf extract of the plant *Camellia sinensis,* also known as tea, have shown to be rich in antioxidant polyphenols, ascorbic acid, and trace elements Cr, Mn, Se, and Zn.[27] Depending on the species, season, and extent of fermentation, the amounts of these health-beneficial compounds can vary significantly. The trace elements Mn, Se, Zn are directly involved with a number of enzymes that reduce oxidative damage.[3] Biological systems use Mn as a constituent for Mn-superoxide dismutase. Additionally, Se serves as a cofactor for glutathione peroxidase, allowing for the removal of peroxide radicals.[3] When considering green, oolong, and fermented teas, green tea has shown to contain a higher content of catechins and other hydroxylated phenols.[27,28] Within green tea, the general trend of quantity of green tea catechins (GTC) is (-)-epigallocatechin gallate (EGCG) > (-)-epicatechin gallate (ECG) > (-)-epicatechin (EC) ≥ (-)-epigallocatechin (EGC) >> (+)catechins.[27,28]

Green Tea Catechins (GTC)

The GTCs are similar in structure, differing only by as many as 2 substitutions (Figure 1-6). The structure of ECG and EC differ only by a gallate present on position 3. EGCG and EGC differ only by an additional hydroxyl group on the B ring in position 5'. Despite these small differences, studies have shown them to differ in various types of

bioactivity and availability. Like many flavonoids, the GTCs have been shown to exhibit potential protective effects against cardiovascular disease, cancer, and neurodegenerative disease.[28]

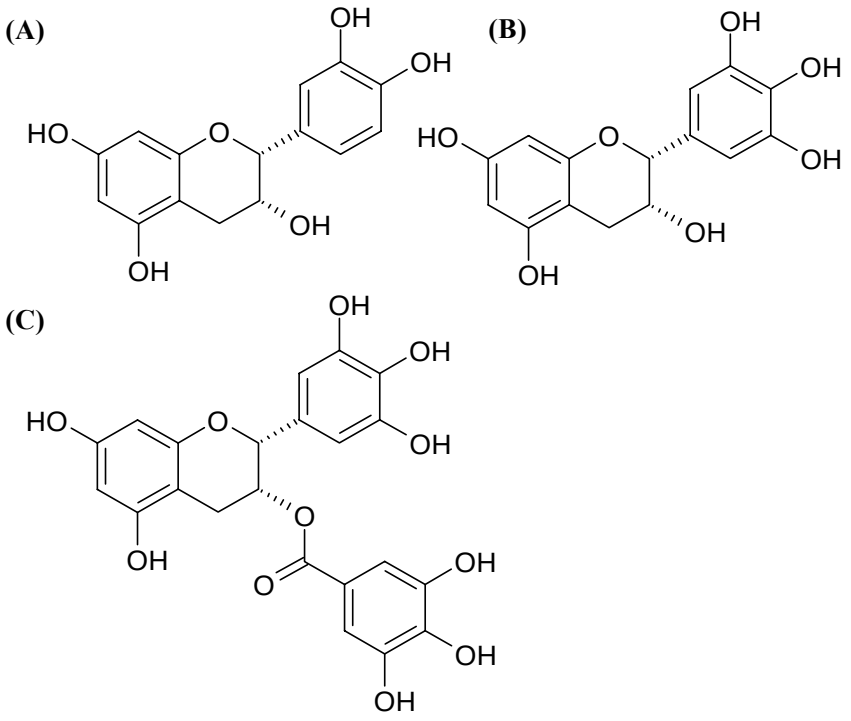

Figure 1-6: The green tea catechins (A) Epicatechin (EC), (B) Epigallocatechin (EGC), (C) Epigallocatechin Gallate (EGCG).

GTCs have gained popularity as they have been demonstrated to show metal chelating, free radical scavenging, protein interaction, and transcription factor regulatory abilities.[23] Specifically, several links have been made between GTCs and diseases involving ROS. Following their reactions with free radicals GTCs form a number of dimers and seven member anhydride rings.[29] In comparison with the body's natural radical scavengers, EGCG can increase cell survival similar to that of catalase in ROS affected cells.[30] Structurally, implications have been made on the advantage of the trihydroxybenzene and gallate moieties to enhance the antioxidant and metal chelation abilities.[23,28] In addition to its chemical properties, the brain-permeability of GTCs may offer beneficial effects in several neurodegenerative diseases. A recent study on Alzheimer's disease has linked EGCG with APP processing.[31] It was shown *in vivo* and *in vitro* that EGCG enhances the activation of the α-secretase and inhibits β-secretase activity, leading more toward a nonamyloidogenic pathway.[31]

Despite their reactivity, there is much concern over the stability of GTCs. Following an oral dose of 100mg of GTCs, only 9-10ug/ml will be absorbed.[26] The absorption deficiency may be due to the change from the acidic stomach to the alkaline blood.[26] In basic conditions, the trihydroxybenzene is probably more susceptible to oxidation and the gallate is hydrolytically cleaved to form gallic acid.[26] Despite these absorption problems, green tea remains one of many good sources of flavonoids.

Citrus Flavonols

Citrus is a flowering plant genus found in the Rutaceae family. It includes fruits such as oranges, grapefruits, and lemons. There is an annual production of 80 million tons of citrus fruits world wide.[32] These fruits are known for their characteristic scent and sharp taste. They are rich both in vitamins and flavonoids. Citrus has utilized these compounds to develop pigmentation and protection from insects in addition to ROS.[22] Studies have linked the components in citrus to prevention of cardiovascular disease, cancers, and allergies.[33] Depending on the fruit, citrus can be an excellent source of many flavonoids. Three structurally similar polyphenols found in citrus are quercetin, fisetin, and taxifolin, which vary in medicinal effect.

Quercetin, Fistein, and Taxifolin

In general, there are several presumed structural requirements for flavonoids to have good antioxidant/antiradical properties. The structural requirements include: a catechol/polyphenol B ring, 2-3 double bond, abundance of free hydroxyl groups, and specifically the 3-hydroxyl group.[34]

Quercetin is the most common flavonol in the human diet. There is an abundance of quercetin in onions, fruits, teas, and red wine.[22] Variations of quercertin are found naturally, having one or more sugars bound at the 3 position. Studies have shown these sugar moieties assist in the absorption of quercetin.[22] Like many flavonoids, queretin bind metal in addition to scavenging free radials.[22,35] Fisetin is a less common flavonol, found in various fruits and vegetables. It differs from quercetin in that it lacks a phenolate. The desaturation of quercetin at the 2-3 position yields taxifolin, appropriately known as dihydroquerctein. Taxifolin is considered a dihydroflavonol and is also found in some fruits and vegetables.[34]

Many studies have compared the flavonoids based on their level of antioxidant and antiradical activity. In a study published by Oleszek et al.[34] the antioxidant properties were found to increase with the presence of the 2-3 double bond (i.e., Quercetin > Fisetin >> Taxifolin). They also showed the antiradical properties were affected by the presence of the 3-OH and not the 2-3 double bond (Taxifolin > Quercetin > Fisetin).[34] As there has been some debate over the "best" flavonoid, it generally agreed upon that the combination of several antioxidants would yield the best antioxidant/radical properties.

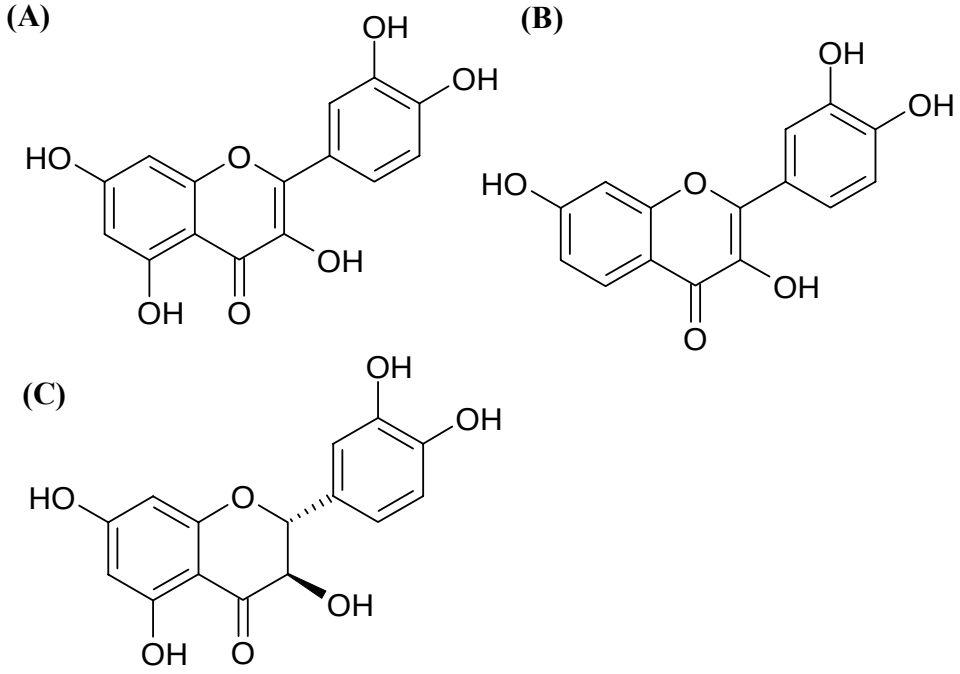

Figure 1-7: Structure of flavonols qercetin (A), fisetin (B), and dihydroflavonol

Vitamins

Once thought to require an amine functional group, they were termed "vital amines" (vitamine). Over the years, structural evidence revealed the lack of the amine in many vitamines, resulting in the loss of the "e" (vitamin).[36] Most vitamins are obtained through the diet and are classified on either being water (B and C) or fat (A, D, E and K) soluble. These compounds are found in abundance in human diet, with fruits and vegetables being excellent sources. Studies have shown that many vitamins have excellent antioxidant properties and are directly involved in many human illnesses.[36]

Vitamin B_6

Considered to be 1 of 8 components of the vitamin B complex, vitamin B_6 is found in three structurally distinct forms: pyridoxal, pyridoxine, pyridoxamine. An enzyme known as pyridoxal kinase converts each of the three in the active form of vitamin B_6, pyridoxal 5'-phosphate.[37] The body utilizes the active form as a cofactor for over 140 enzymes.[37] Some of which are involved in amino acid and monoamine neurotransmitter synthesis.[38] A deficiency in vitamin B_6 has been shown to lead to insufficient insulin and altered hormone production.[38] The recommended daily intake is 2 mg, which is easily obtained from various vegetables, fish, and non-citrus based fruit.[38] In addition to its regulatory roles vitamin B_6 has also been shown to serve as a potent antioxidants.[39] Studies have suggested that components of vitamin B_6 inhibit the product of radicals and serve as quenchers for singlet oxygen.[39]

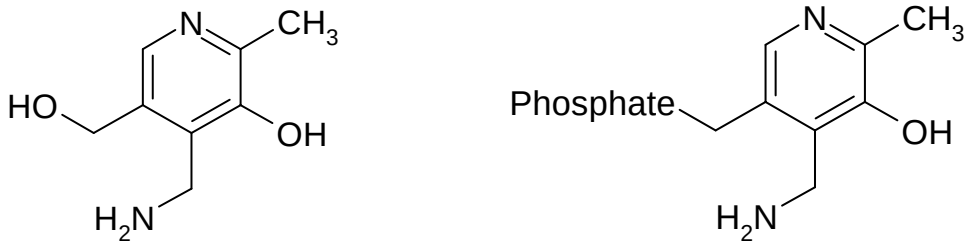

Figure 1-8: Structures of pyridoxamine and pyridoxamine-5'-phosphate

Ascorbic Acid

Being the most abundant soluble antioxidant in plants, L-ascorbic acid (AsA) (aka. Vitamin C) (Figure 1-9) has become increasingly consumed because of its proposed health benefits.[40] At risk of diseases such as scurvy, AsA is considered essential in the human diet. The body uses AsA as radical scavenger, calcium regulator, and as a cofactor for multiple enzymes, some involved in collagen synthesis. It is the antioxidant/antiradical properties associated with AsA have believed to be responsible for its contribution to the prevention of numerous chronic diseases.[40]

Through consumption of beverages such as green tea, one can easily obtain the recommended daily intake of 30-110 mg/day.[40] In addition to its health benefits, AsA effect on the absorption of other biological components has also been measured.[26] For example, the low absorption of GTCs is thought to be because of its oxidative breakdown. Results have shown AsA to serve as a reductant that can protect GTCs and potentially increase their total absorption.[26] Although the overall effect of one compound

can be significant, it is usually thought that a combination of antioxidants (e.g. flavonoids and vitamins) can provide a more beneficial antioxidant protective effect.[41]

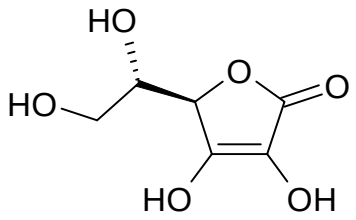

Figure 1-9: Structure of (*R*)-3,4-dihydroxy-5-((*S*)-1,2-dihydroxyethyl)furan-2(5*H*)-one (Ascorbic Acid)

Closing Remarks:

When characterizing an enzyme, it is not uncommon to use model systems to reveal both mechanistic and structural information. Furthermore, it is often beneficial to find stable enzyme mimics that exhibit high levels of activity. This thesis presents both modeled and natural peptides that show tyrosinase-like activity. The former is the metzinicin active site and is characterized through metal binding, activity, and inhibition. The latter are varied fragments of Alzheimer's disease-related amyloid-β. Catalytic efficiency and mechanistic insight are obtained on amyloid through the use of physiologically relevant substrates. In addition, select flavonoids and vitamins are used to show that the possible consumption of high content antioxidant foods can reduce oxidative stress caused by Aβ. These antioxidants are compared based on their overall effect of the Aβ tyrosinase-like chemistry.

References:

1) McMurry, J.; Fay, R. *Chemistry*, 3rd Edition; Prentice-Hall: New Jersey, 2001.

2) Voet, D.; Voet, J. Biochemistry, 3rd Edition; John Wiley & Sons: New Jersey, 2004.

3) da Silva, F., and Williams, R. *The biological chemistry of the elements.* 2nd edition. Oxford University Press, 2000.

4) Vincent, B. (2000) Elucidating a Biological Role for Chromium at a Molecular Level. J. Acc. Chem. Res., 33, 503-510

5) Wolfram, B., Franz-Xaver, G., and Walter, S. (1993) Astacins, serralysins, snake venom and matrix metalloproteinases exhibit identical zinc-binding environments (HEXXHXXGXXH and Met-turn) and topologies and should be grouped into a common family, the'metzincins' FEBS Letters., 331, 134-140.

6) da Silva, F. Z. G., Reuille, L, R., Ming, L., and Livingston, T, B. (2006) Overexpression and Mechanistic Characterization of Blastula Protease 10, a Metalloprotease Involved in Sea Urchin Embryogenesis and Development. J. Biol. Chem., 281, 16, 10737-10744.

7) Hyun, P. and Ming, L. (1998) The mechanistic role of the coordinated tyrosine in astacin. J. Inorganic Biochem., 72, 57-62.

8) Hyun, P. and Ming, L. (2002) Mechanistic studies of the astacin-like Serratia metalloendopeptidase serralysin: highly active (>2000%) Co(II) and Cu(II) derivatives for further corroboration of a "metallotriad" mechanism. J. Biol. Inorg. Chem., 7, 600-610.

9) Gaggelli, E,. Kozlowski, H,. Valensin, D,. and Valensin G. (2006) Copper homeostasis and neurodegenerative disorders (Alzheimer's, prion, and Parkinson's diseases and amyotrophic lateral sclerosis). Chem. Rev., 106, 1994-2044.

10) Mirica, M, L., Ottenwaelder, X., and Stack, P, D. (2004) Structure and spectroscopy of copper-dioxygen complexes Chem. Rev., 104, 1013-1045.

11) Soloman, I, E., Sundaram, M, U., and Machonkin, E, T. (1996) Multicopper Oxidases and Oxygenases Chem. Rev. , 96, 2563-2605.

12) Ferrari,P., Laurenti, E., Ghibaudi, M, E., and Casella, Luigi. (1997) Reversible Dioxygen Binding and Phenol Oxygenation in a Tyrosinase Model System. J. Inorg. Biochem., 68, 61-69.

13) Selmeczi, K., Reglier, M., Giorgi, M., and Speier,G. (2003) Catechol oxidase activity of dicopper complexes with N-donor ligands. Coordination Chem. Rev., 245, 191-201.

14) Mahadevan, V., Gebbink, K, R., and Stack, T, D. (2000) Biomimetic modeling of copper oxidase reactivity. Curr. Opin. Chem. Bio., 4, 228-234.

15) Boka, B., Myari, A., Sovago, I., and Hadjiliadis, N. (2004) Copper(II) and zinc(II) complexes of the peptides Ac-HisValHis-NH2 and Ac-HisValGlyAsp-NH2 related to the active site of the enzyme CuZnSOD. J Inorg Biochem., 98,113-22.

16) CDC.gov

17) Huang, X., Moir, D, R., Tanzi, E, R., Bush, I, A., and Rogers, T, J. (2004) Redox-Active Metals, Oxidative Stress, and Alzheimer's Disease Pathology. Ann. N.Y. Acad. Sci. 1012, 153-163.

18) Chong, Z, Z., Li, F., and Maiese, K. (2005) Employing New Cellular Therapeutic Targets for Alzheimer's Disease: A Change for the Better?. Curr. Neurovascular Research, 2, 55-72.

19) da Silva, F, Z, G., Tay, M, W., and Ming, L. (2005) Catechol Oxidase-like Oxidation Chemistry of the 1–20 and 1–16 Fragments of Alzheimer's Disease-related β-Amyloid Peptide. J. Bio. Chem., 280, 17, 16601-16609.

20) Mekmouche, Y., Coppel, Y., Hochgräfe, K., Guilloreau, L., Talmard, C., Mazarguil, H., and Faller, P. (2005) Characterization of the Zn II Binding to the Peptide Amyloid-b linked to Alzheimer's Disease. Chem. Bio. Chem., 6, 1663-1671.

21) Gnanakaran, S.; Nussinov, R.; Garcia, A. E. (2006) Atomic-Level Description of Amyloid β-Dimer Formation. J. Am. Chem. Soc. 128(7); 2158-2159.

22) Erlund, I. (2004) Review of the flavonoids quercetin, hesperetin, and naringenin. Dietary sources, bioactivities, bioavailability, and epidemiology. Nutrition Research, 24, 851-874.

23) Mandel, S., Amit, T., Reznichenko, L., Weinreb, O., and Youdim, M. (2006) Green tea catechins as brain-permeable, natural iron chelators-antioxidants for the treatment of neurodegenerative disorders. Nutr. Food Res, 50, 229-234.

24) Casetta, I., Govni, V., and Granieri E. (2005) Oxidative stress, antioxidants and neurodegenerative diseases. Curr. Pharm. Des., 2005;11: 2033-52.

25) Furusawa, M., Tanaka, T., Ito, T., Nishikawa, A., Yamazaki, N., Nakaya, K., Matsuura, N., Tsuchiya, H., Nagayama, M., and Iinuma, M. (2005) Antioxidant Activity of Hydroxyflavonoids. Journal of Health Science, 51(3), 376-378.

26) Chen, Z., Zhu, Y, Q., Wong, F, Y., Zhang, Z, and Chung, H. (1998) Stabilizing effect of ascorbic acid on green tea catechins. J. Agric. Food Chem., 46, 2512-2516.

27) Cabrera, C., Gimenez, R., and Lopez, M. C. (2003) Determination of tea components with antioxidant activity J. Agric. Food Chem, *51*, 15, 4427-4435.

28) Zaveri, Nurulain. (2006) Green tea and its polyphenolic catechins: medicinal uses in cancer and noncancer applications. Life Sci., 78, 2073-2080.

29) Valcic, S., Muders, A., Jacobsen, E, N., Liebler, C, D., and Timmermann, N, B. (1999) Antioxidant Chemistry of Green Tea Catechins. Identification of Products of the Reaction of (-)-Epigallocatechin Gallate with Peroxyl Radicals. Chem. Res. Toxicol., 12, 382-386.

30) Choi, Y., Jung, C., Lee, S., Bae, J., Baek, W., Suh, M., Park, J., Park, C., and Suh, S. (2001) The green tea polyphenol (-)-epigallocatechin gallate attenuates beta-amyloid-induced neurotoxicity in cultured hippocampal neurons. Life Sciences, 70, 603-614.

31) Rezai-Zadeh, K., Shytle, D., Sun, N., Mori, T., Hou, H., Jeanniton, D., Ehrhart, J., Townsend, K., Zeng, J., Morgan, D., Hardy, J., Town, T., and Tan J. (2005) Green Tea Epigallocatechin-3-Gallate (EGCG) Modulates Amyloid Precursor Protein Cleavage and Reduces Cerebral Amyloidosis in Alzheimer Transgenic Mice**.** J. of Neuroscience 25, 38, 8807-8814.

32) Bocco, A., Cuvelier, M., Richard, H., and Berset, C. (1998) Antioxidant Activity and Phenolic Composition of Citrus Peel and Seed Extracts. J. Agric. Food Chem., 46, 2123-2129.

33) Croft, D, K. Annals NY Academy of Sci. (1998) The Chemistry and Biological Effects of Flavonoids and Phenolic Acids. 854, 435-441.

34) Burda, S. and Oleszek, W. (2001) Antioxidant and Antiradical Activities of Flavonoids. J. Agric. Food Chem., 49, 2774-2779.

35) Thompson, M. and Williams, C. R. (1976) Antioxidant Potential of Ecklonia cavaon Reactive Oxygen Species Scavenging, Metal Chelating, Reducing Power and Lipid Peroxidation Inhibition. Analytica Chimica Acta, 85, 375-381.

36)Asard, H., May, J,. and Smirnoff, N. Vitamin C Functions and biochemistry in animals and plants. Garland Science: New York, 2004.

37) Tang, L., Li, M., Cao, P., Wang, F., Chang, W., Bach, S., Reinhardt, J., Ferandin, Y., Galons, H., Wan, Y., Gray, N., Meijer, L., Jiang, T., Liang, D. (2005) Crystal Structure of Pyridoxal Kinase in Complex with Roscovitine and Derivatives. J. Bio. Chem., 280, 35, 31220-31229.

38) Dolphin, D., Poulson, R., Avramovic, O.Vitamin B6 Pyridoxal Phosphate, Volume 1. 1986, John Wiley & Sons.

39) Yokochi, N., Morita, T., Yagi, T. (2003) Inhibition of Diphenolase Activity of Tyrosinase by Vitamin B_6 Compounds. J. Agric. Food Chem., 51, 2733-2736.

40) Viola, R. and Hancock, R. (2005) Biosynthesis and Catabolism of L-Ascorbic Acid in Plants. J. Agric. Food Chem. 53, 5248-5257.

41) Saucier, T, C. and Waterhouse, L, A. (1999) Synergetic Activity of Catechin and Other Antioxidants. J. Agric. Food Chem. 47, 4491-4494.

Chapter Two

Blastula Protease-10 Peptide as Tyrosinase-like Mimic

Introduction/ Rationale

Blastula Protease 10 (BP10) is a mono-nuclear Zn-dependent endopeptidase that is involved in sea urchin embroyogenesis.[1] The enzyme utilizes a structural motif (HE*xx*H*xx*G*xx*H) and a Tyr ligand following a distant "Met turn" to coordinate the Zn^{2+} ion. These conserved structures are found in nearly 30 different enzymes and are classified as "metzinicins."[2] The exact role of BP10 in embroyogenesis is still unknown. Furthermore, it is difficult to make comparisons to other members of the metzincins because each differs remarkably in localization. In a recent study, the copper derivatives of BP10 was prepared and have been shown to be more hydrolytically active in comparison to that of the native Zn-derivative.[1] The binding of Cu^{2+} to the His rich motif has alluded to the possibility of additional types of Cu-chemistry.

For years, model complexes have been prepared to characterize both intermediates and mechanisms for Type 3-Copper proteins, such as Tyrosinase.[3,4] Tyrosinase is an enzyme found in both plants and animals, responsible for the synthesis of melanin. This enzyme is well studied partially due to its agricultural significance, specifically its role in the browning of food. These model complexes tend to be nitrogen rich and activity is usually shown in mixed organic/aqueous solvent.[3] Only in the past few years have begun to use model peptides to mimic enzymatic catalysis.[5,6] The next chapter will concern the use of the metzincin motif from BP10 as tyrosinase mimic in aqueous media. Metal binding and mechanistic information is alluded to by various kinetic experiments.

Experimental:

Chemicals and Materials for Metal Titrations and Kinetics Assays:

The BP10 peptide was synthesized and purchased from the University of South Florida Peptide Center. The identity of the 21 amino acid peptide (GIVHE IGHAI GFHHE QSAPD R) was confirmed with a Bruker matrix-assisted laser desorption ionization MALDI time-of-flight mass spectrometer. The buffer used in all assays is 100 mM HEPES at pH 7, with small amount of chlex resin to demetalize the solution. EDTA was used in cleaning glass/plastic ware prior to usage in order to prevent metal contamination. Deionized water of 18 MΩ was obtained from a Milli Q system (Millipore, Bedford, MA) and used for all cleaning and for preparation of stocks solutions. $CuSO_4$ and $ZnSO_4$ were used for all experiments. All kinetic studies were run using a Varian CARY50 Bio-UV-Vis spectrophotometer at 293 K.

Peptide Preparation

The molar absorptivity was determined by monitoring the absorbance of known concentrations of peptide dissolved in water at 280nm for phenylalanine. Metal derivatives were prepared by the addition of a known concentration of metal to achieve a 1:1 ratio of metal to peptide. Fresh peptide stocks were prepared and used within 24 hours.

Metal Binding

Apo-BP10 was diluted in 100 mM HEPES at pH 7.00 to a final concentration of 0.5 mM. The binding of Cu^{2+} was monitored by titrating metal into apo-BP10 and collecting the spectra after each additional of metal. Cu^{2+} binding was also determined

through oxidative activity of Cu^{2+}-BP10 complex toward catechol. In 100 mM HEPES pH 7.00 buffer, 2mM catechol, and the 2 mM o-quinone indicator 3-methyl-2-benzothiazolinone hydrazone hydrochloride monohydrate (MBTH), activities of various ratios of Cu:BP10 were monitored at 500nm for the o-quninone-MBTH complex (Figure 2-1). Additionally, Cu^{2+}/Zn^{2+} at various ratios were titrated to BP10 and the oxidation of catechol (conditions same as Cu^{2+} titration) monitored.

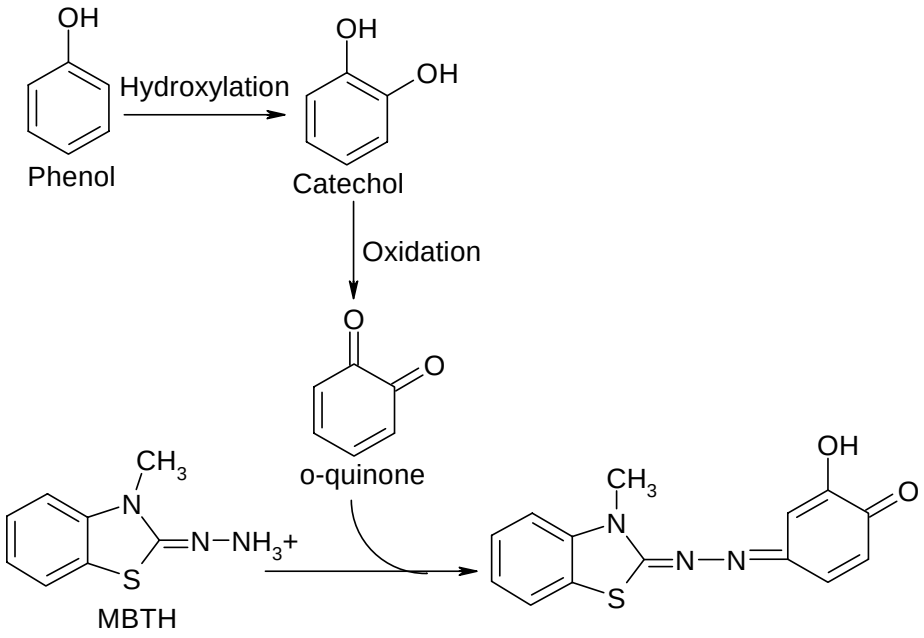

Figure 2-1: Scheme showing the binding of o-qunione indicator 3-methyl-2-benzothiazolinone hydrazone hydrochloride monohydrate (MBTH)

Enzyme Kinetics

The study of the effect of changing experimental conditions on the rate of an enzyme-catalyzed reaction is known as enzyme kinetics. In most studies, the initial rate, V_o, varies almost linearly with substrate concentration, [S] is determined. At higher [S], V_o response is decreased, eventually being virtually unaffected by any addition of S. This seemingly constant rate is considered as the maximum velocity, V_{max}. The reaction between the enzyme, E, and S, yields an ES complex, a necessity for the next step in enzymatic catalysis.

$$\mathbf{E + S} \underset{\mathbf{k_{-1}}}{\overset{\mathbf{k_1}}{\rightleftharpoons}} \mathbf{ES} \xrightarrow{\mathbf{k_2}} \mathbf{E + P}$$

When the enzyme is initially introduced to the substrate, the reaction quickly achieves a steady state, with the ES complex remaining constant over time. The ES complex then breaks down to yield a product (P) and an E that is able to catalyze another reaction. The breakdown of the ES complex is used to determine V_o (Equation 2.1).

$$V_o = k_2[ES] \qquad \text{Equation 2.1}$$

Experimentally it is difficult to determine [ES], making it important to consider alternative methods to determine V_o. Utilizing a steady-state assumption that states the [ES] complex is formed and broken-down at an equivalent rate, one can derive an equation that can determine V_o though the use of experimentally derived parameters. The rate of ES formation and breakdown can be define by equations (Equation 2.1, 2.2)

$$\frac{d[ES]}{dt} = k_1([E_t] - [ES])[S] \qquad \text{Equation 2.2}$$

$$\frac{-d[ES]}{dt} = k_{-1}[ES] + k_2[ES] \qquad \text{Equation 2.3}$$

Where $[E_t]$ is the total enzyme concentration (both in E and ES). Setting these equivalent and through some algebraic manipulation to solve for [ES], yields Equation 2.4.

$$[ES] = \frac{[E_t][S]}{[S] + \frac{(k_2 + k_{-1})}{k_1}} \qquad \text{Equation 2.4}$$

By substituting equation 2.4 into equation 2.1, one can express the equation in terms of V_o (Equation 2.5).

$$V_o = \frac{k_2[E_t][S]}{[S] + \frac{(k_2 + k_{-1})}{k_1}} \qquad \text{Equation 2.5}$$

Because V_{max} is defined as the maximum velocity attained after the enzyme is saturated (Equation 2.6), the equation to solve for V_o can further be simplified (Equation 2.7)

$$V_{max} = k_2[E_t] \qquad \text{Equation 2.6}$$

$$V_o = \frac{V_{max}[S]}{[S] + \frac{(k_2 + k_{-1})}{k_1}} \qquad \text{Equation 2.7}$$

Another parameter of particular importance is the Michaelis-Menten constant (K_m). This is usually defined as the substrate concentration that has a rate equal to half the V_{max}. K_m is solved to give Equation 2.8.

$$K_m = \frac{k_2 + k_{-1}}{k_1} \qquad \text{Equation 2.8}$$

Substituting this equation in equation 2.7 yields what is known as the Michaelis-Menten equation (Equation 2.9) and is depicted in figure 2-2.

$$V_o = \frac{V_{max}[S]}{K_m + [S]}$$ Equation 2.9

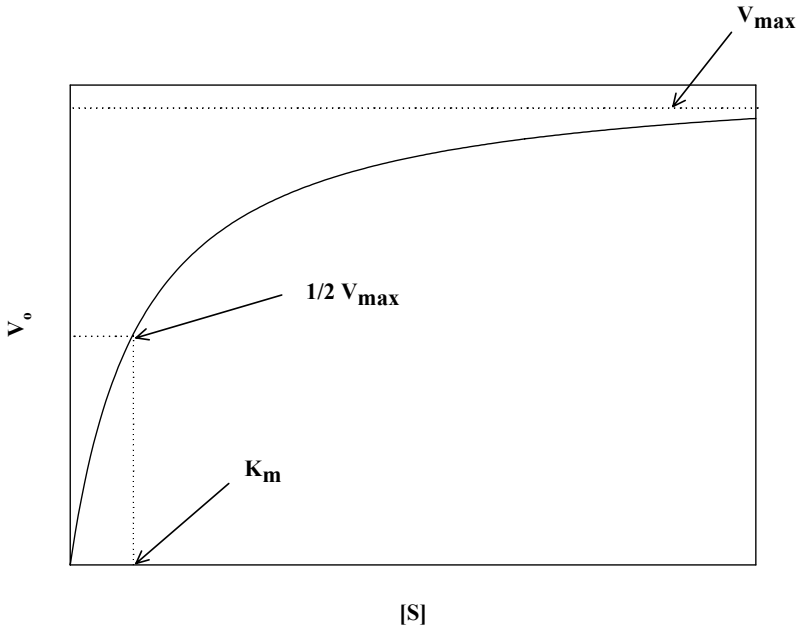

Figure 2-2: Michaelis-Menten plot.

Depending on the rate limiting step, specifically when $k_2 << k_{-1}$, K_m can be used to represent the affinity of E to S in the ES complex. When this condition holds, K_m is defined as the dissociation constant (K_d) (Equation 2.10), of the ES complex.

$$K_d = \frac{k_{-1}}{k_1}$$ Equation 2.10

Since enzymes can react in fashions that the rate limiting step is not the degradation of ES, the first-order rate constant k_{cat} is often used to report rates in terms of turnover per time (Equation 2.11).

$$k_{cat} = \frac{V_{max}}{[E]}$$ Equation 2.11

Furthermore, to compare enzymes the second order rate constant k_{cat}/K_m (specificity constant) is used to describe the conversion of E + S to E + P.

Another common technique to determine kinetic parameters is through the use of a double-reciprocal or Lineweaver-Burk plot (Equation 2.12, Figure2-3).

$$\frac{1}{V_o} = \frac{K_m}{V_{max}[S]} + \frac{1}{V_{max}} \qquad \text{Equation 2.12}$$

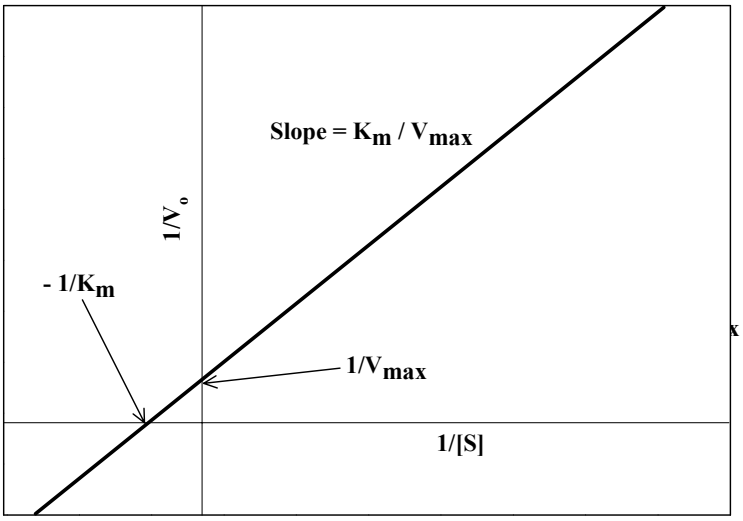

Figure 2-3: Lineweaver-Burk plot.

The Lineweaver-Burk plot is particularly useful to distinguish types of inhibition patterns, including competitive, noncompetitive, uncompetitive, and mixed-type inhibition. A competitive competes for the active site of an enzyme with the substrate. This direct competition of the inhibitor (I) can be overwhelmed by increasing amounts of

S. This type of inhibition has a trend of increasing K_m and relativity constant V_{max}. Competitive inhibition is depicted by the scheme, equations, and plot in Figure 2-4.

$$\frac{1}{V_o} = \frac{K_m}{V_{max}} \frac{1}{[S]} \left(1 + \frac{[I]}{K_i}\right) + \frac{1}{V_{max}}$$

$$E + S \underset{k_{-1}}{\overset{k_1}{\rightleftharpoons}} ES \xrightarrow{k_2} E + P$$

$$E + I \rightleftharpoons EI \quad (K_i)$$

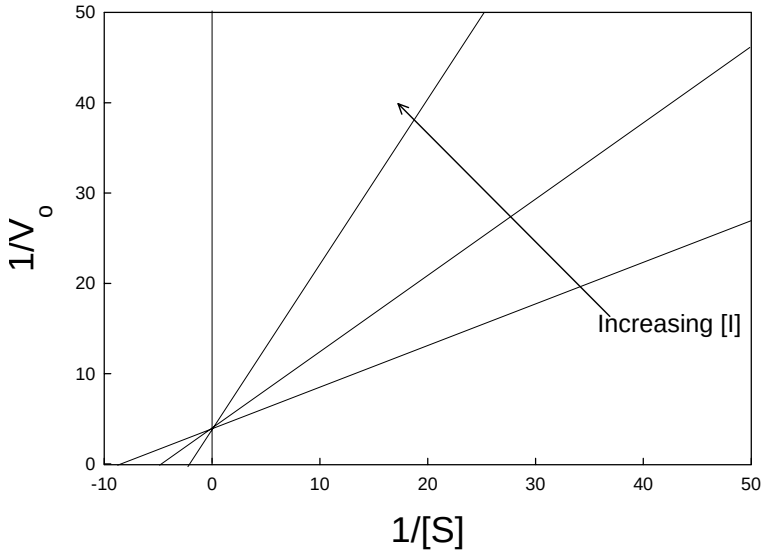

$$\frac{1}{V_o} = \frac{K_m}{V_{max}} \frac{1}{[S]} (1 + \frac{[I]}{K_i}) + \frac{1}{V_{max}}$$

Figure 2.4: Graphical, schematic, and equations for competitive inhibition

Another type of inhibition, considered noncompetitive, is when the inhibitor binds both E and the ES. This type of inhibition usually has the trend of increasing V_{max} and constant K_m. This type of inhibition is shown by the following Lineweaver-Burk plot trend and equations in figure (2-5).

$$V = \frac{V_{max}[S]}{([S] + K_m)(1 + [I]/K_i)}$$

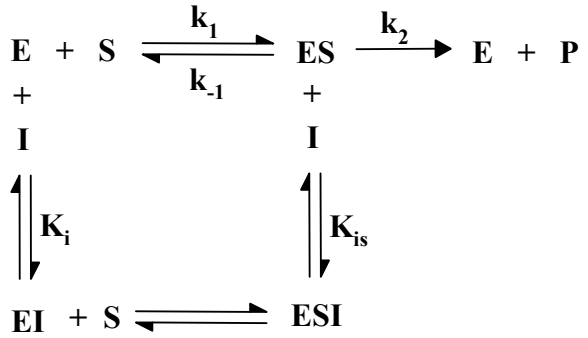

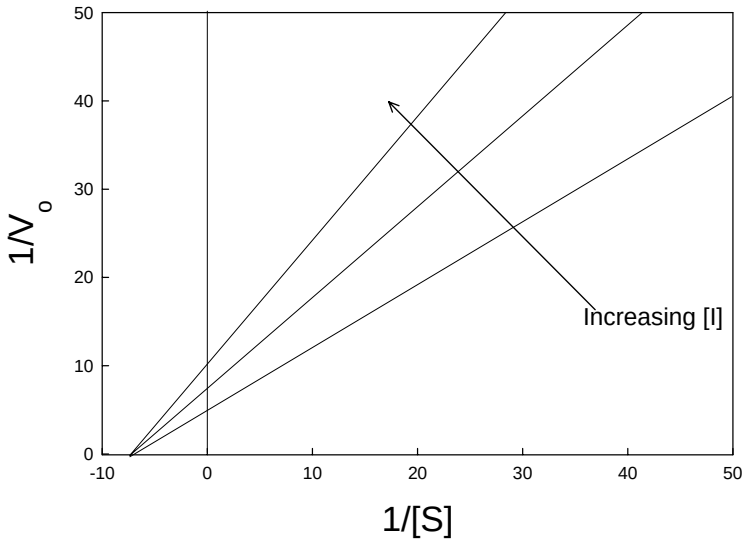

Figure 2.5: Graphical, schematic, and equations for noncompetitive inhibition

A third type of inhibition is a mix between competitive and non-competitive, appropriately named mixed type. Mixed type inhibition is the same equilibrium as noncompetitive, with inhibitor binding at different affinities to both the E and ES complex. (Figure 2.6)

$$\frac{V_{max(app)}}{K_{m(app)}} = \frac{\frac{V_{max}}{K_m}}{1 + \frac{[I]}{K_i}} \qquad V_{max(app} = \frac{V_{max}}{1 + \frac{[I]}{K_{is}}}$$

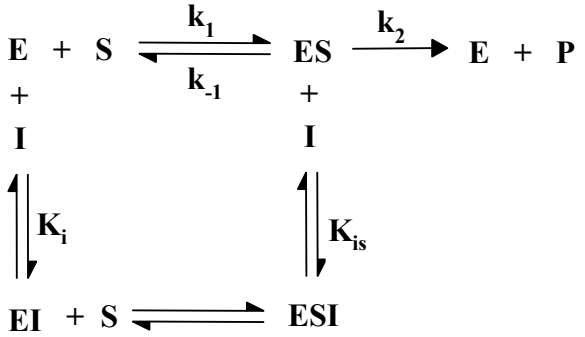

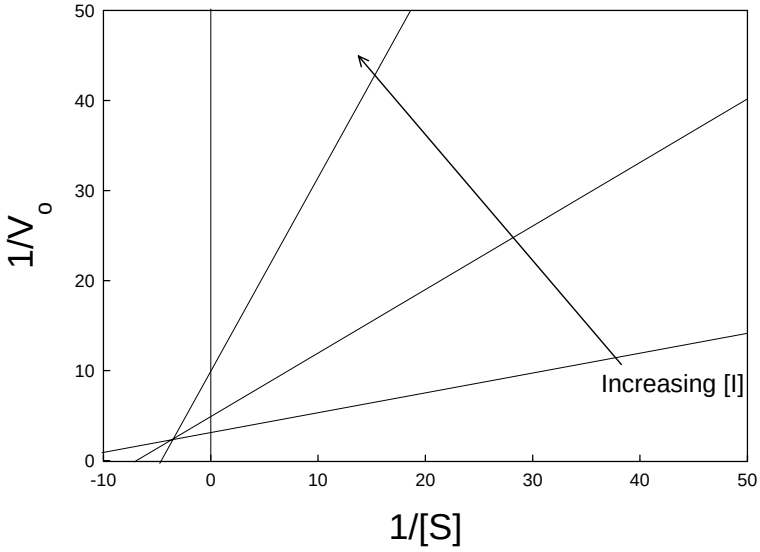

Figure 2.6: Graphical, schematic, and equations for mixed-type inhibition.

The forth type of inhibition which is when the inhibitor binds only to the ES complex. An inhibitor is considered to be uncompetitive when it influences the rate by binding to a location other then substrate binding site. The binding to the ES complex is associated with decreasing K_m and V_{max}. (Figure 2.7)

$$V_o = \frac{V_{max}\,[S]}{K_m + [S]\left(1 + \frac{[I]}{K_i}\right)}$$

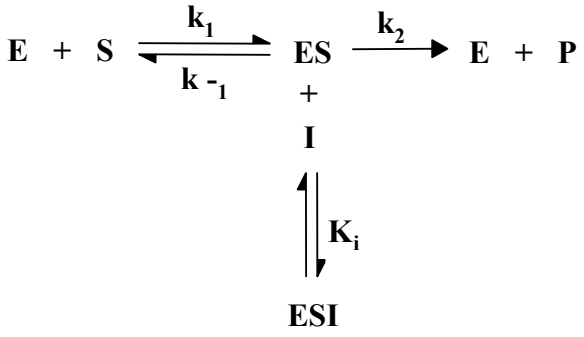

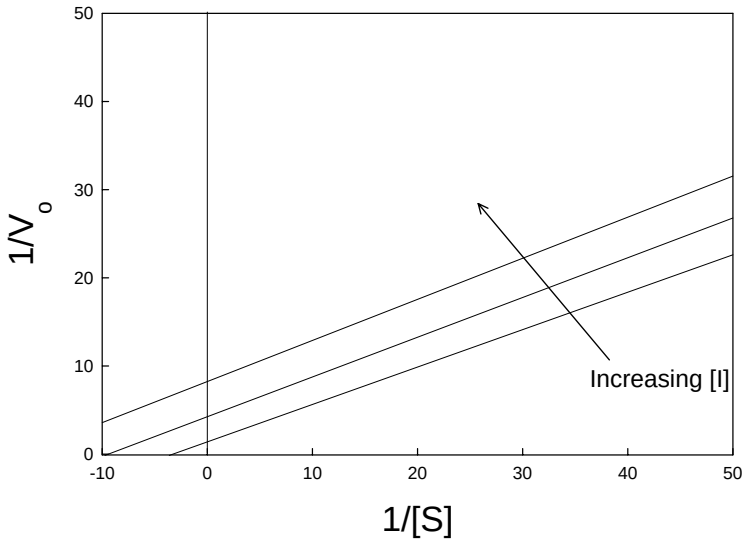

Figure 2.7: Graphical, schematic, and equations for uncompetitive inhibition

Catechol/Phenol oxidation Assays

Using a constant Cu-BP10 concentration (2-10μM) with a 1:1 Cu to peptide ratio, various substrate concentrations were assayed. The final volume of each assay is 1 mL at pH 7.00 100 mM HEPES and 298 K. The concentration of MBTH was kept in proportion with substrate concentration. Catechol was varied 0.05-1.2 mM and the MBTH-o-quinone product was monitored at 500 nm for 3-5 mins (Figure 2-8A) The rates were determined by the change in absorbance over time (Figure 2-8B). A similar assay was constructed for phenol with concentrations ranging from 0.2-3.2 mM and was also monitored at 500 nm for o-quinone production.

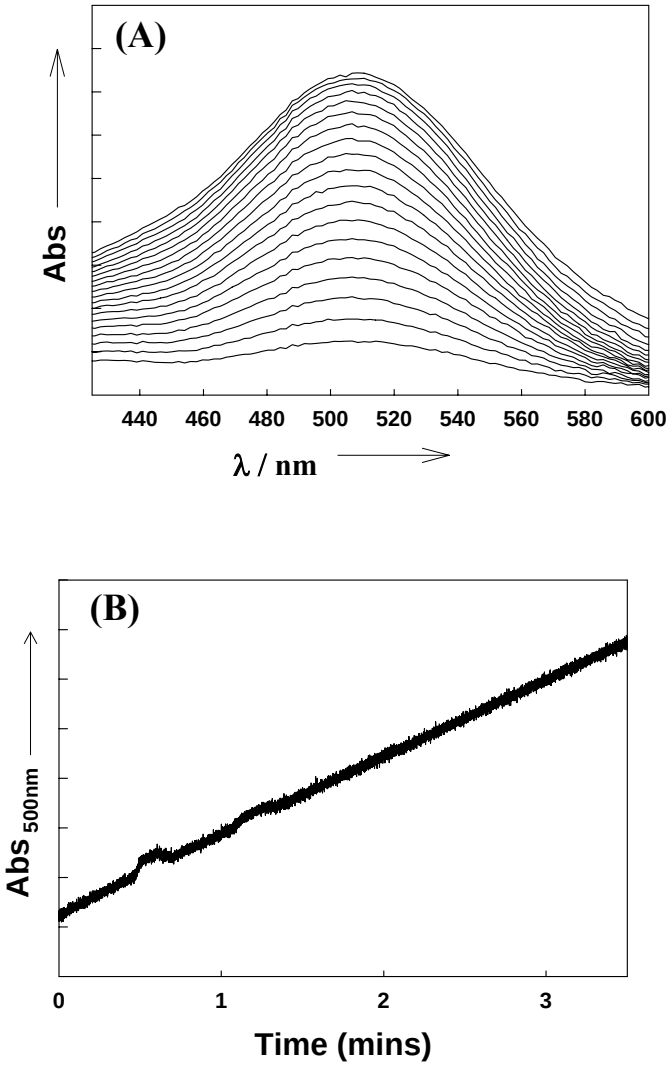

Figure 2-8: (A) The production of o-quinone from catechol monitored by the increase in absorption as a result of the formation of its adduct with 3-methyl-2-benzothiazolinone hydrazone hydrochloride monohydrate (MBTH). (B) Monitoring the increase in absorption at 500 nm for catechol oxidation to obtain the rate.

Hydrogen peroxide (H_2O_2) titration was perfomed with fixed catalyst and saturating amount of substrate. The conditions were similar to non-H_2O_2 assays described above. H_2O_2 varied from 0.25mM-12mM and the catechol/phenol-MBTH product (ε = 32,500 M^{-1} cm^{-1}) was monitored at 500 nm. Additionally, experiments were

preformed that varied catechol concentration at a fixed catalyst and H_2O_2 concentration. The assays preformed had a [H_2O_2] fixed at 0.25, 0.75, 1.5, 3.0, or 6.0 mM.

Deuterated–phenol (d-phenol) experiments were performed under the same conditions as described above. Using 10 μM Cu^{2+}-BP10 and varying *d*-phenol from .4-3.2 mM the absorbance was monitored at 500 nm. Furthermore, under saturating conditions of H_2O_2 (20 mM), d-phenol was titrated.

Inhibition Experiments

Conditions for inhibition experiments consisted of 0.5-2 μM Cu^{2+}-BP10, pH 7.00, 100 mM HEPES buffer, 293 K, and 1 ml total volume. To obtain the Dixon plot, kojic acid was titrated into assays containing fixed catechol and MBTH concentrations (0.3mM). Kojic acid concentration varied from 0.025 - 0.8 mM. Catechol oxidation was then monitored at various concentrations of kojic acid (0.25, 0.05, and 0.1 mM) at 500 nm.

Cyanide inhibition was monitored under similar conditions to kojic acid inhibition. A dixion plot was obtained by titrating cyanide into a fixed amount of catechol (0.3mM) and monitoring for the formation of the o-qunione. Catechol oxidation was then monitored at various concentrations of cyanide (0.002,0.005, 0.0035, mM) to obtain the Lineweaver-Burk plot. A Dixon plot was then obtained that kept catechol, MBTH, catalyst, and H_2O_2 (0.7 mM) constant, while titrating cyanide. Assays were then performed at 0, 0.015 and 0.03 mM cyanide, while varying H_2O_2 from 0.125-10 mM. A third inhibition experiment was preformed that varied catechol at various cyanide concentrations (0, 0.015, 0.03 mM) while keeping H_2O_2 under saturating condition (8 mM).

Results and Discussion

Metal Binding

To examine the metal-coordination environment, the electronic spectrum of Cu^{2+}-BP10 was obtained (Figure2.5). Upon the addition of Cu^{2+}, there is a d-d transition with a λ_{max} of 610 nm. The spectrum is analogous to type-2 copper centers and distinct from aqueous Cu^{2+} absorbance at 820 nm.[6] Furthermore the spectrum is comparable to published Cu^{2+}-bound His-rich peptides.[6] In order to gain further insight into the metal-centered redox chemistry, activity was also used to confirm the Cu^{2+}:BP10 stoichiometry. By measuring the activity at various equivalents of Cu^{2+}, the resulting data saturates around 1:1 ligand-to-metal ratio (Figure 2.6). The data reveals a sigmoidal pattern which is fit to the Hill equation yielding a Hill coefficient of 2.87. In general, a Hill coefficient greater then unity indicates a positive cooperatively. For comparsion purposes, the coefficient for Cu^{2+} binding to BP10 is equivalent to that of O_2 binding to hemoglobin with a Hill Coefficient of 2.8. To gain further insight into the metal-center, diluting Cu^{2+}-BP10 with Zn^{2+} would effectively silence the redox chemistry. If the catalysis is carried out by a mononuclear Cu^{2+}-center, the Zn^{2+} should replace the Cu^{2+} and result in a non-cooperative nearly linear binding. Figure 2.6 indicates a sigmodal relationship, yielding a Hill coefficient of 1.76. This suggests the possible presence of a cooperative Cu^{2+} binding to form a Type-3 copper center during the catalysis of catechol, corroborating with the result in direct Cu^{2+} binding (Figure 2.,6 Top)

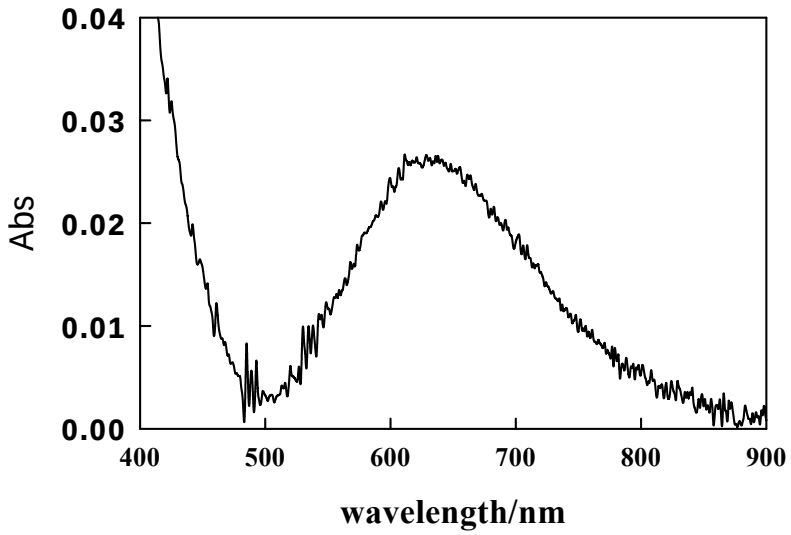

Figure 2.9: Electronic spectra of Cu^{2+}-BP10 with 1 equivalent of Cu^{2+}-BP10. (100 mM HEPES buffer at pH 7.0, 0.5 mM BP10)

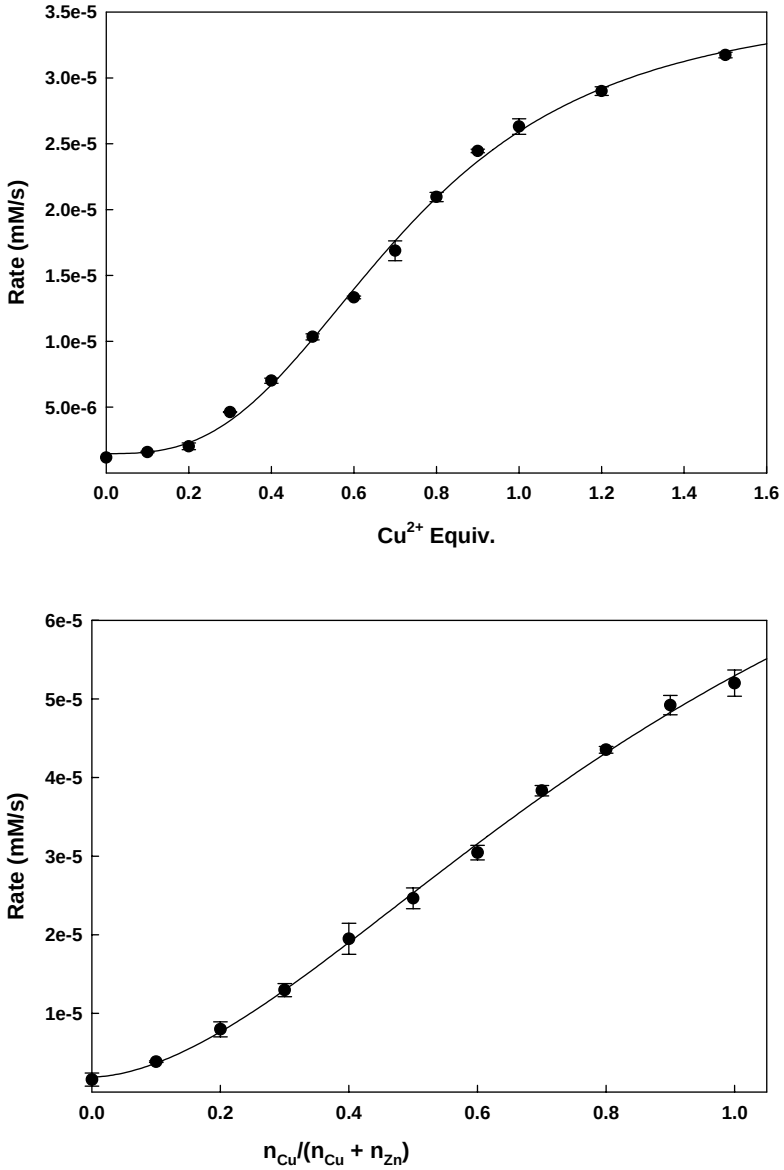

Figure 2.10: (Top) Cu^{2+} titration to BP10 monitored with the oxidation of catechol. Fit to Hill equation, which yields a Hill coefficient of 2.86 ± 0.18. (Bottom) Oxidative activity of Cu^{2+}-BP10 toward the oxidation of catechol as a function of the mole fraction of Cu^{2+} at a constant total concentration of Cu^{2+} and Zn^{2+}. Fit to Hill equation, which yield Hill coefficient of 1.76 ± 0.17. (Both assays contained [BP10] = 6 μM, [MBTH] = [catechol] = 2mM, 100 mM HEPES buffer pH 7.0, 293 K)

Catechol/Phenol Oxidation

The oxidation of catechol to o-quinone is a 2-electron transfer that favors the presences of a dinuclear Cu^{2+} center. Studies concerning tyrosinase and catechol oxidase have shown that once the dinuclear center is in the met form, catechol can readily bind and be oxidized to its quinone product.[7] In the presence of O_2, micromolar amounts of Cu^{2+}-BP10 can readily oxidize catechol and is saturated at mM amounts of substrate (Figure 2.7), yielding a $k_{cat} = 4.06\ s^{-1}$, $K_m = 0.254$ mM, and a significant second-order rate constant of $1.60 \times 10^4\ M^{-1}\ s^{-1}$. In terms of first order rate constant, Cu^{2+}-BP10 is 8.57×10^6 fold higher than the autooxidation of catechol ($k_o = 4.74 \times 10^{-7}\ s^{-1}$) and 7.5 fold higher then another catechol oxidizing peptide mimic ($0.531\ s^{-1}$).[6]

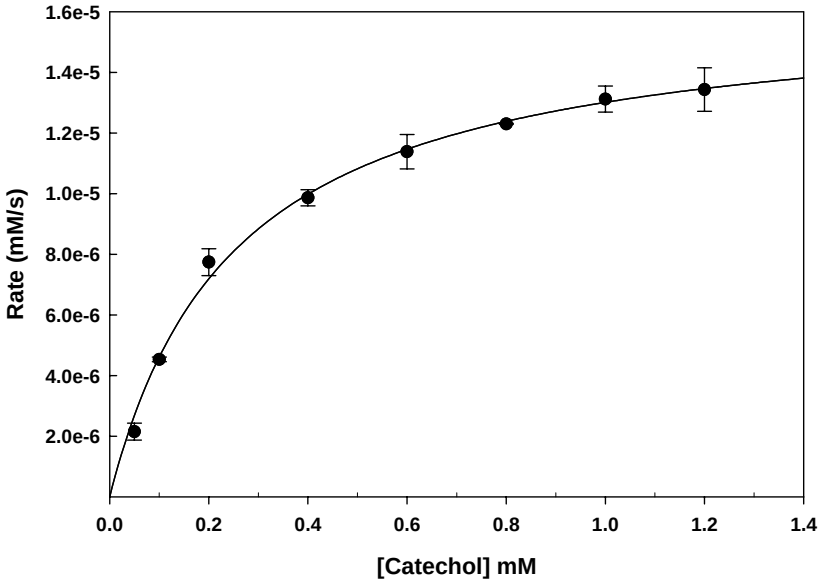

K_m	(mM)	0.254 ± .020
V_{max}	(mM/s)	(1.63 ± .04) x 10^{-5}
k_{cat}	(s^{-1})	4.06
k_{cat}/K_m	(mM^{-1} s^{-1})	16.0

Figure 2.11: Cu^{2+}-BP10 oxidation of catechol at pH 7.00 and 293K. [Cu^{2+}-BP10] kept constant at 4 μM. Table includes kinetic parameters.

To gain further insight into the mechanism of Cu^{2+}-BP10, H_2O_2 was titrated into the complex with saturating amounts of catechol (Figure2.8). The data showed a significant increase in rate and was saturated after mM amounts of H_2O_2. The saturation kinetics observed for both catechol and H_2O_2 implies a possible bisubstrate mechnaism, wherein both can bind to the metal active center. To obtain apparent and

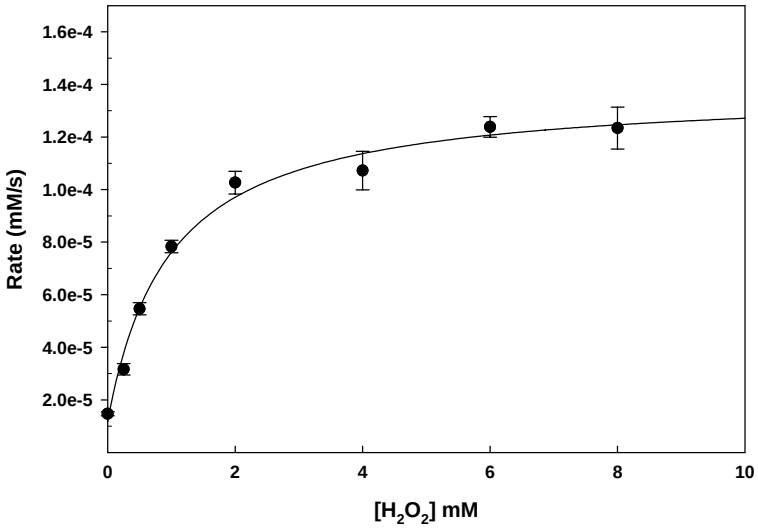

K_m	(mM)	.967 ± .188
V_{max}	(mM/s)	$1.27x10^{-4} \pm 6.12x10^{-6}$
k_{cat}	(s^{-1})	31.8
k_{cat}/K_m	(mM^{-1} s^{-1})	32.8

Figure 2.12 The effect of H_2O_2 on Cu^{2+}-BP10 oxidation of catechol in the presence of saturating catechol (1.5mM) at pH 7.00 and 293K. [Cu^{2+}-BP10] kept constant at 4uM. Table includes kinetic parameters.

intensic dissociation constants for catechol and H_2O_2, the rates at varying amounts of $[H_2O_2]$ holding [catechol] constant and vise versa were determined (Figure 2.9). The data could be fitted to a two-substrate random-binding equilibrium shown below.

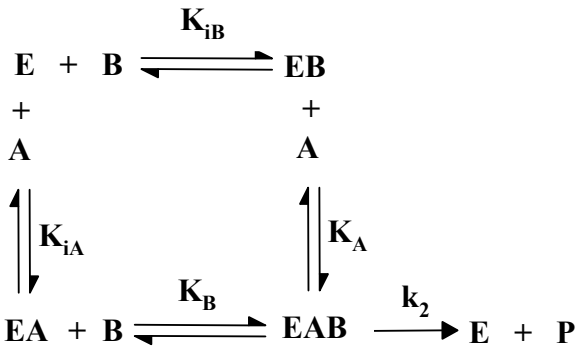

$$\frac{\text{Catechol}}{V_o} = \frac{1}{V_{max}} + \frac{K_{app(H)}}{V_{max}[H_2O_2]}[\text{Catechol}] + \frac{K_{app(C)}}{V_{max}} + \frac{K_{app(C)}K_{int(C)}}{[H_2O_2]}$$

Figure 2-13: Random bisubsubstrate equation and equilibrium.

In the equation, $K_{app(H)}$ is the apparent affinity constant for H_2O_2, $K_{app(C)}$ is the apparent affinity constant for catechol, and $K_{int(C)}$ is the intrinsic affinity constant for catechol. From the Hanes analysis, a secondary plot of the slope ($1/V_{max}$) and the y-intercept ($K_{app(Substrate)}/V_{max}$) verus 1/[Substrate] is obtained (Figure 2.10). From the slopes and y-intercepts of these secondary plots, the apparent and intensic dissociation constants can be obtained. Using the ratios of K_{app}/K_{int} the effect of the binding of one substrate on the other can be measured. If the ratio is above 1, then the binding of one ligand decreases the affinity for the other, below one represents an increased affinity, and equal to 1 indicates no effect on one another. From the results obtained

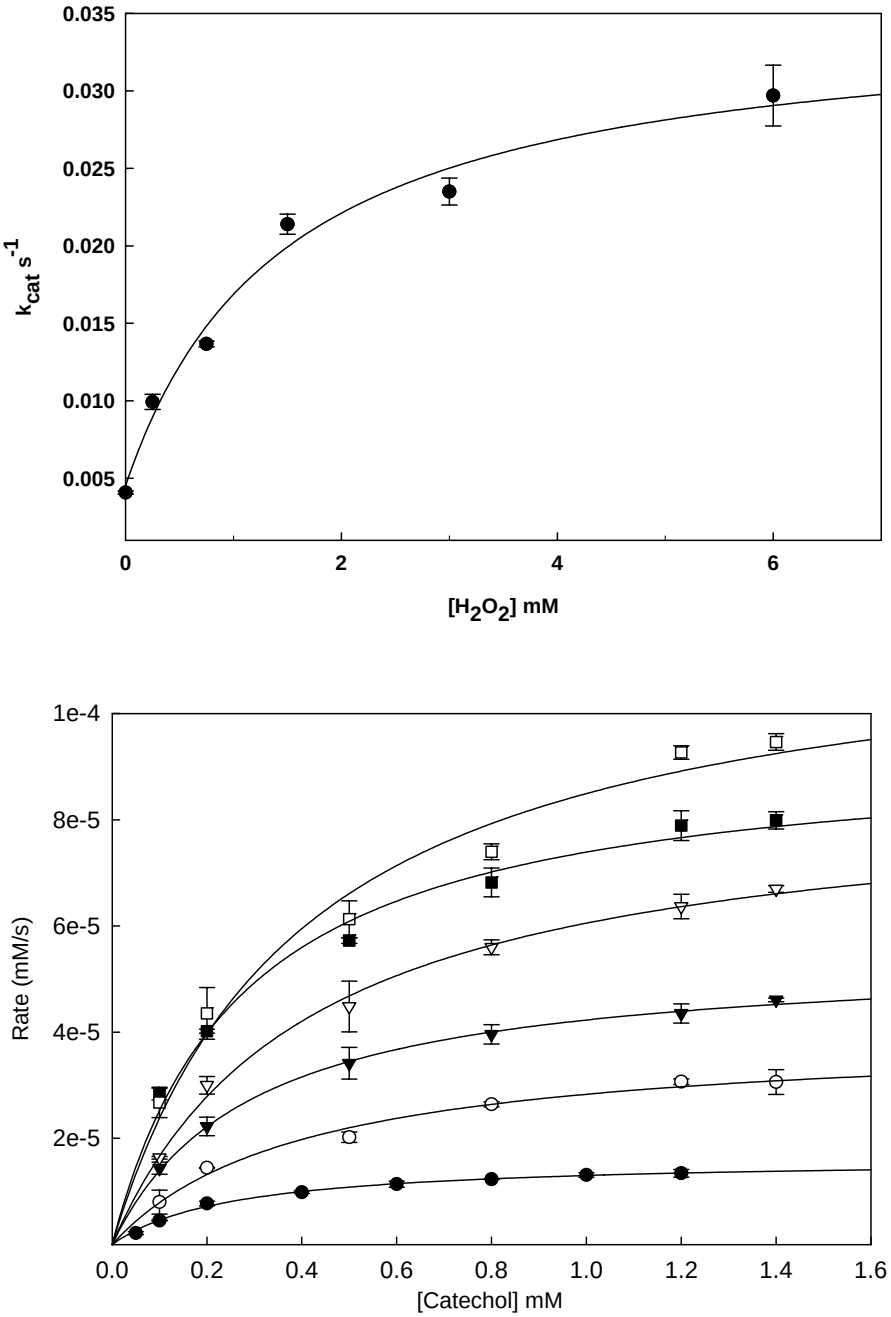

Figure 2.14: (Top Plot) The effect of the concentration of H_2O_2 on the first-order rate constant k_{cat} toward the Cu^{2+}-BP10 oxidation of catechol. (Bottom Plot) 0 (●), 0.25 (○), 0.75 (▼), 1.5 (Δ), 3.0 (■), and 6 mM (□) H_2O_2 effect on the rate of catechol oxidation. Conditions at pH 7.0 and 293 K, [Cu^{2+}-BP10] = 2 µM.

$K_{app(C)}/K_{int(C)}$ =0.752, while $K_{app(H)}/K_{int(H)}$ = 1.04. From the Hanes analysis, catechol seems to have no effect on H_2O_2 binding, while H_2O_2 increases the affinity for catechol slightly. Although these results provide insight into the Cu^{2+}-BP10 mechanism, alone they provide insufficient evidence to conclude the sequencal binding.

In addition to catechol oxidation, Cu^{2+}-BP10 was shown to hydroxylate and oxidize phenol to the o-qunione product. Phenol hydroxylation is often times challenging for metal-centered chemistry because it is a spin-forbidden process, inserting the triplet O_2 into the singlet C-H bond. Furthermore, the aerobic hydroxylation/oxidation of phenol is relativity slow ($k_0 = 4.60 \times 10^{-8}\ s^{-1}$).[6] Cu^{2+}-BP10 was shown to significantly enhance the tyrosinase-like hydroxylation activity by 8.57×10^3 times ($k_{cat} = 3.94 \times 10^{-4}\ s^{-1}$). The rate compared to catechol oxidation is significantly reduced by around 1×10^5 times, believed to be in part due to the difficult hydroxylation step. To further inquire if in fact the rate determining step is the hydroxylation, d-phenol was used as a substrate. The rate of the reaction remained relatively unchanged, with a kinetic isotope effect of only 1.27. This result indicates that hydroxylation is most likely not the rate determining step of the reaction.

[H2O2] mM	K_m (mM)	V_{max} (mM/s)	k_{cat} (s^{-1})	k_{cat}/Km ($M^{-1}\ s^{-1}$)
0	0.25 ± 0.02	$(1.63 \pm 0.04) \times 10^{-5}$	4.06	16.0×10^3
0.25	0.40 ± 0.06	$(3.97 \pm 0.20) \times 10^{-5}$	19.9	49.4×10^3
0.75	0.29 ± 0.01	$(5.47 \pm 0.08) \times 10^{-5}$	27.4	93.5×10^3
1.5	0.41 ± 0.04	$(8.56 \pm 0.26) \times 10^{-5}$	42.8	103×10^3
3.0	0.27 ± 0.03	$(9.40 \pm 0.35) \times 10^{-5}$	47.0	173×10^3
6.0	0.39 ± 0.08	$(1.19 \pm 0.78) \times 10^{-4}$	59.5	149×10^3

Table 2.1: Kinetic parameters for H_2O_2 effect on Cu^{2+}-BP10 oxidation of catechol.

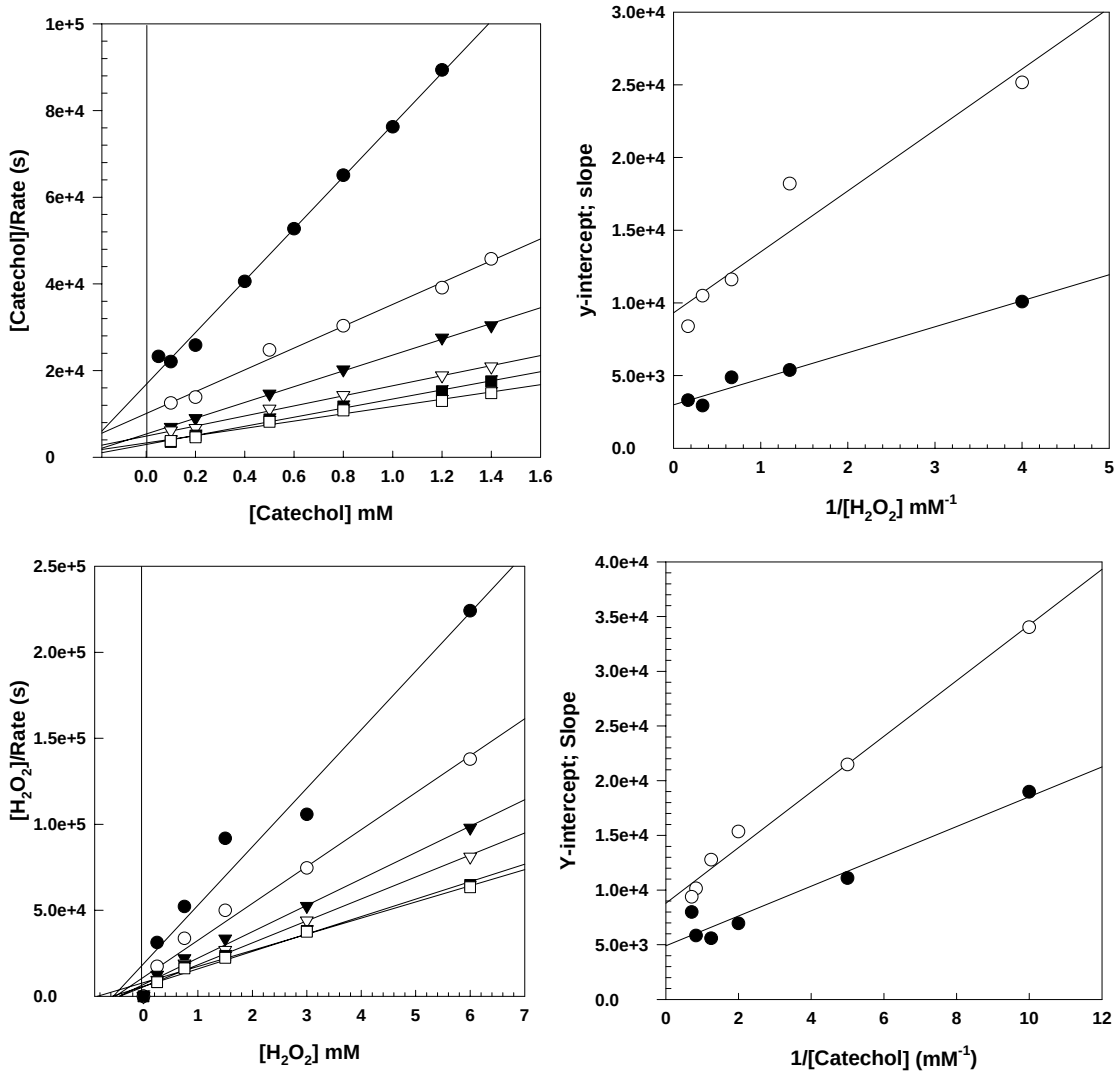

$K_{m\ (C)}$ (mM)	0.427
$K_{app\ (C)}$ (mM)	0.321
$K_{m\ (H)}$ (mM)	0.535
$K_{app\ (H)}$ (mM)	0.558
$K_{app\ (H)} / K_{m\ (H)}$	1.04
$K_{app\ (C)} / K_{m\ (C)}$	0.752

Figure 2.15: (Top) Hanes analysis of various [catechol] and secondary plot (slope ○, y-intercept ●). (Bottom) Hanes analysis of various [H_2O_2] and secondary plot (slope ○, y-intercept ●). Table includes apparent and intrinsic affinity constants for catechol and H_2O_2.

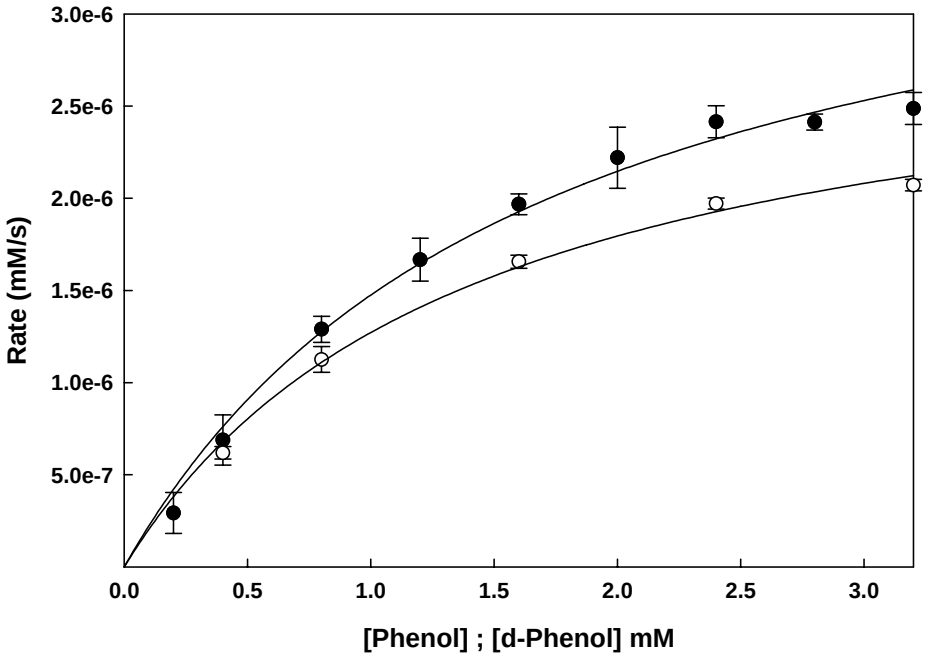

	Phenol	*d*-Phenol
K_m (mM)	1.67 ± .218	1.40 ± .176
V_{max} (mM/s)	(3.9 ± 0.2) x 10^{-6}	(3.1 ± 0.2) x10^{-6}
k_{cat} (s^{-1})	3.94x10^{-4}	3.05x10^{-4}
k_{cat}/K_m (mM^{-1} s^{-1})	2.36x10^{-4}	2.18x10^{-4}

Figure 2-16: Cu^{2+}-BP10 hydroxylation/oxidation of phenol (●) and d-phenol (○) without H_2O_2. Table includes kinetic parameters.

Inhibition

The results thus far have indicated that both H_2O_2 and catechol/phenol are substrates for Cu^{2+}-BP10. Further detailed mechanistic inferences can be made by the use of oxygen and catechol mimics as inhibitors. A popular competitive inhibitor for Type-III Cu-centers is kojic acid.[8] As seen in Figure 2-12, kojic acid shows to be a competitive inhibitor for catechol oxidation by Cu^{2+}-BP10. The low K_i indicates the inhibitor has tight binding and is relatively specific for the catalyst. Kojic acid inhibition further supports the notion of the presence of a dinuclear center and that catechol binds to the same location as kojic acid.

To gain insight into the role and binding of the oxygen species cyanide was used as an inhibition. Cyanide is a well-known oxygen mimic that has been used to characterize O_2 binding sites. In figure 2-13, cyanide is used in the presence of atmospheric O_2 while titrating catechol. The mixed type inhibition and near equal K_i and K_{is} indicate cyanide binds to both the E and ES complex with similar affinity. Since the concentration of O_2 in solution is unknown and may not be at saturating conditions, the type of inhibition for this assay reveals only the possible presence competitive and uncompetitive inhibition and that cyanide can bind to the E and/or ES complex. Another cyanide inhibition assay checked the inhibition in the presence of saturating conditions of catechol while titrating H_2O_2 (Figure 2-14). The results reveal a clear noncompetitive pattern between cyanide and H_2O_2. The inhibitor in noncompetitive inhibition binds both the E and the ES complex. Being that catechol is at saturating conditions and bound first to E, cyanide could possibly serve as a reducing agent stabilizing and blocking Cu^+ and thus preventing O_2 from binding. The third cyanide inhibition experiment involved H_2O_2

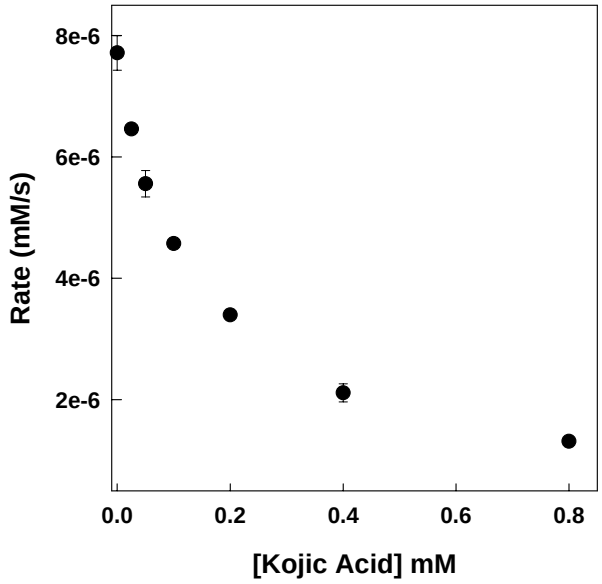

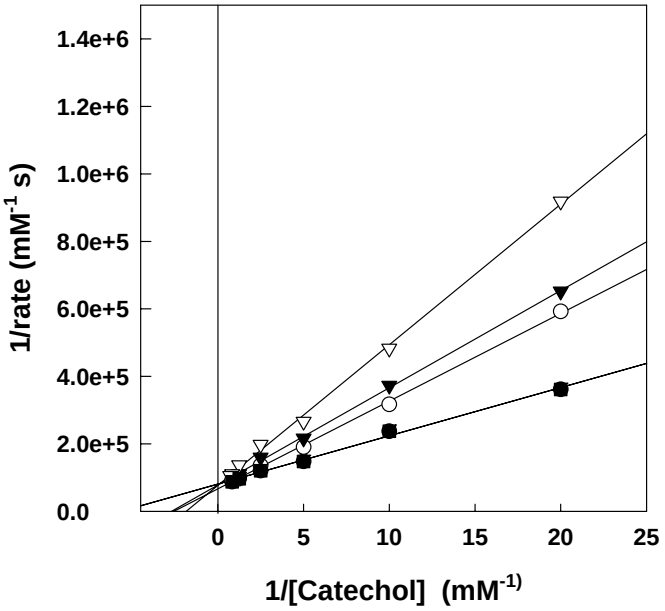

[Kojic Acid] mM	K_m (mM)	V_{max} (mM/S)
0.00	0.202 ± .016	(1.30 ± 0.03) x 10^{-5}
2.50e-2	0.344 ± .013	(1.39 ± 0.02) x 10^{-5}
5.00e-2	0.435 ± .041	(1.39 ± 0.05) x10^{-5}
1.00e-1	0.534 ± .074	(1.28 ± 0.07) x 10^{-5}
K_i= 0.043 mM		

Figure 2-17: Kojic Acid Inhibition- (Top) Kojic acid titration into constant [catechol] and [Cu^{2+}-BP10]. (Bottom) Lineweaver-Burk plot titrating catechol at different [kojic acid] (0 mM, ●; 0.025 mM,○; 0.05 mM, ▼; 0.10 mM, Δ) (Table) The effects of [kojic acid] on V_{max} and K_m, in addition to the K_i for competitive inhibition.

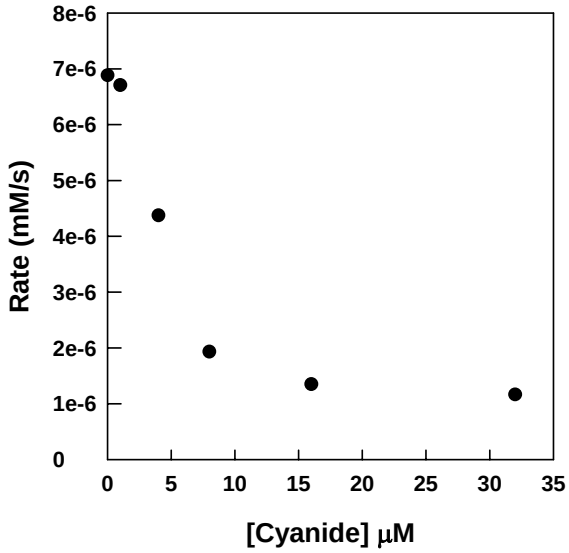

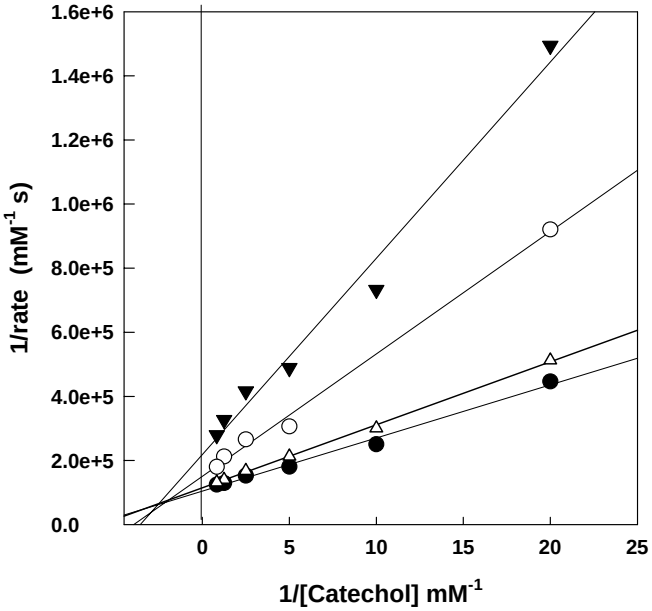

[Cyanide] mM	K_m (mM)	Vmax (mM/s)
0.00	0.132 ± .008	(8.96 ± 0.16) x 10^{-6}
5.0 x 10^{-4}	0.166 ± .005	(8.59 ± 0.08) x 10^{-6}
2.0 x10^{-3}	0.211 ± .034	(6.22 ± 0.33) x 10^{-6}
3.5 x 10^{-3}	0.223 ± .035	(4.06 ± 0.21) x 10^{-6}
K_i = (1.4 ± 1.7) x10^{-3} mM | K_{is} = (6.3 ± 4.7) x10^{-3} mM		

Figure 2-18: Cyanide Inhibition in the presence of O_2. (Top) Cyanide titration into constant [catechol] and [Cu^{2+}-BP10]. (Bottom) Lineweaver-Burk plot titrating catechol at different [cyanide] (0 mM●, 0.5μM Δ, 2.0 μM ○, 3.5 μM ▼) (Table) The effects of [cyanide] on V_{max} and K_m, in addition to the K_i (Interaction with free E) and K_{is} (interaction with the ES complex) for mixed type inhibition.

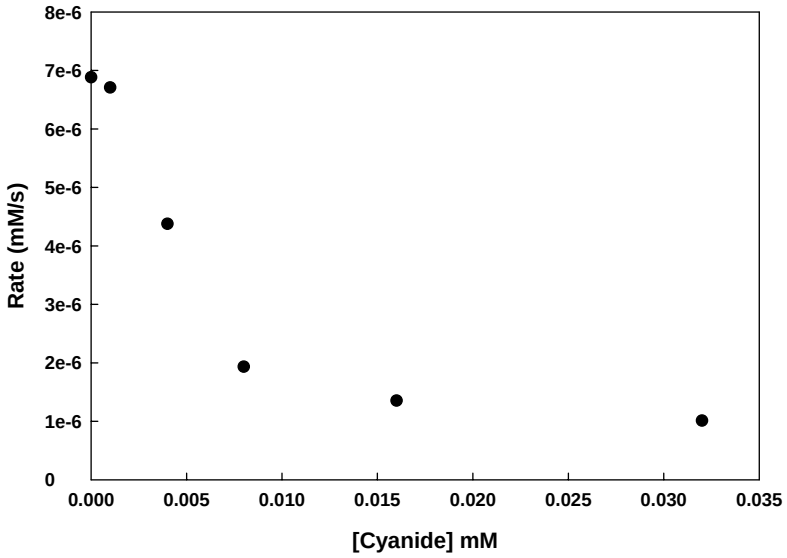

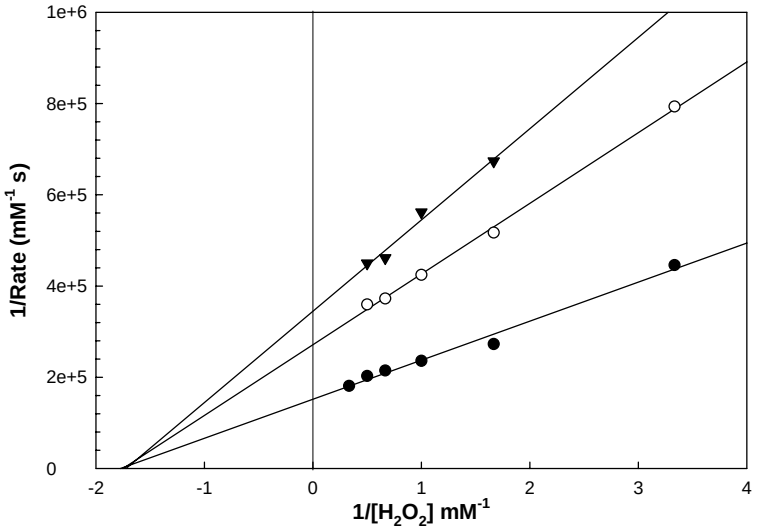

[Inhibitor] mM	K_m (mM)	V_{max} (mM/s)
0.0	0.496 ±.052	(6.31 ± 0.19) x 10^{-6}
1.5 x 10^{-3}	0.522 ± .034	(3.57 ± 0.08) x 10^{-6}
3.0 x 10^{-3}	0.764 ± .137	(3.17 ± 0.23) x 10^{-6}
K_i= 3.03x10^{-3} mM		K_{is}= 1.45x10^{-3} mM

Figure 2-19: Cyanide Inhibition in the presence of H_2O_2. (Top) Titrating cyanide into fixed [Catechol], [Cu^{2+}-BP10], and [H_2O_2]=.7mM. (Bottom) Lineweaver-Burk plot titrating H_2O_2 at different [cyanide] (0 mM,●; 1.5 µM, ○; 3.0 µM, ▼) while keeping [catechol] at saturating conditions. (Table) The effects of [cyanide] on V_{max} and K_m, in addition to the K_i for noncompetitive inhibition.

binding. The third cyanide inhibition experiment involved H_2O_2 at saturating conditions while titrating catechol (Figure 2-15). The results clearly represents uncompetitive inhibition of cyanide against catechol. An uncompetitive inhibitor binds only to the ES complex. Since cyanide is considered an oxygen mimic, the results suggest that oxygen (cyanide) would bind to the active center after catechol is bound to form the Cu^{2+}-BP10-catechol complex.

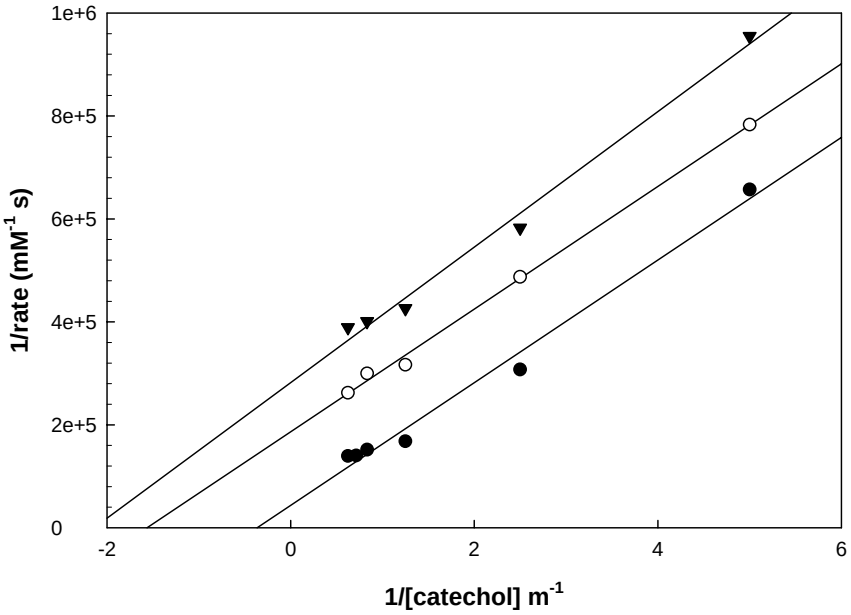

[Inhibitor] mM	K_m (mM)	V_{max} (mM/s)
0.0	1.06 ± 0.28	(1.24 ± 0.16) x10^{-5}
1.5 x 10^{-3}	.590 ± 0.085	(5.19 ± 0.94) x 10^{-6}
3.0 x 10^{-3}	.375 ± 0.053	3.27 ± 0.15) x10^{-6}
K_i = 1.64 x 10^{-3} mM		

Figure 2-20: Cyanide Inhibition in the presence of H_2O_2. Lineweaver-Burk plot titrating catechol at different [cyanide] (0 mM●, 1.5 μM ○, 3.0 μM ▼) while keeping [H_2O_2] at saturating conditions (8mM). (Table) The effects of [cyanide] on V_{max} and K_m, in addition to the K_i.

Closing Remarks

The metzinicin motif found in BP10 has shown to bind Cu^{2+} and form a Type-III Cu-center. The complex is relatively active in comparison to the background rate of catechol and phenol oxidation. Furthermore, it shows that H_2O_2 can enhance the reaction and serves as the second substrate in a bisubstrate reaction. From the Hanes analysis, catechol seems to have no effect on H_2O_2 binding, while H_2O_2 increases the affinity for catechol slightly. The catechol binding to the free E was confirmed by the kojic acid inhibition. Cyanide inhibitions confirmed that oxygen is involved in the reaction and that cyanide binds only after catechol binding.

Reference

1) Da Silva, GFZ. Reuille, L, R., Ming, L., and Livingston, T. (2006) Overexpression and Mechanistic Characterization of Blastula Protease 10, a Metalloprotease Involved in Sea Urchin Embryogenesis and Development. J. Biol. Chem., 281, 16, 10737-10744.

2) Bode, W., Gomis-Rueth, FX., and Stoeckler, W. (1993) Astacins, serralysins, snake venom and matrix metalloproteinases exhibit identical zinc-binding environments (HEXXHXXGXXH and Met-turn) and topologies and should be grouped into a common family, the 'metzincins', FEBS Letters, 331, 134-140.

3) Granata, E., Monzani, and Casella, L. (2004) Mechanistic insight into the catechol oxidase activity by a biomimetic dinuclear copper complex. J. Biol. Inorg. Chem. 9, 903-913.

4) Mahadevan, W., Gebbink, RK., and Stack, TDP. Curr. Opin. Chem. Bio. (2000) Biomimetic modeling of copper oxidase reactivity. 4, 228-234.

5) Casolaro, M., Chelli, M., Ginanneschi, M., Laschi, F., Messori, L., Muniz-Miranda, M., Papini, AM., Kowalik-Jankowska, T., and Kozlowski, H. (2002) Spectroscopic and potentiometric study of the SOD mimic system copper(II)/acetyl-L-histidylglycyl-L-histidylglycine. J. Inorg. Biochem. , 89, 181-90.

6) Da Silva, GFZ., Tay, WM., and Ming, L. (2005) Catechol Oxidase-like Oxidation Chemistry of the 1-20 abd 1-16 Fragments of Alzheimer's Disease-Related β-Amyloid Peptide: Their Structure-Activity Correlation and the Fate of Hydrogen Peroxide. J. Bio. Chem., 280, 16601-16609.

7) Soloman, I, E., Sundaram, M, U., and Machonkin, E, T. (1996) Multicopper Oxidases and Oxygenases Chem. Rev., 96, 2563-2605.

8) Chen, J., Cheng-I Wei, C., Marshall, M. (1991) Inhibition Mechanism of Kojic Acid on Polyphenol Oxidase? J. Agric. Food Chem., 39, 1897–1901.

Chapter Three

Alzheimer's Disease and Natural Antioxidants

Introduction/ Rationale

Of neurodegenerative diseases, the most prevalent is Alzheimer's disease (AD). Although the past decade has made significant progress on the cause of the disease, it still remains somewhat of a mystery. Of the many hypotheses proposed, the common link seems to be amyloid β-peptide (Aβ).[1] This short peptide varies in length following secreatase cleavage of the amyloid precursor protein (APP).[1] In general, shorter more soluble fragments are considered to be nonamyloidgenic, while longer hydrophobic fragments are considered the cause or effect of AD.[1] Along with a microtubule stabilizing tau protein, longer fragments of Aβ have shown to accumulate, forming plaques in the brain.[1] Studies have shown these plaques to be responsible for alterations in normal brain function, such as abnormal Ca^{2+} homeostasis and production of H_2O_2.[1,2,3] Furthermore, postmortem studies have revealed the presence of redox active metal (e.g. Cu^{2+}) present in the plaques.[4] The presence of this seemingly misguided metal has fueled the hypothesis of reactive oxygen species (ROS) as a major component of neuronal cell loss. In addition, studies have shown Aβ to bind metal with a relativity high affinity within the first 14 amino acids of the peptide.[5]

This study presents soluble fragments of Cu^{2+}-bound Aβ as highly redox active complexes. Compassions between fragments of Aβ containing the amino acids believed to start dimerization will be examined.[6] This will include the effect of ROS on the redox activity of Cu^{2+}-Aβ toward the neurotransmitter dopamine. In addition, natural antioxidants (e.g. flavonoids and vitamins) will be used to inhibit this AD-related redox

chemistry. This will allow for further infancies on the possible beneficial effect of numerous antioxidants and the identification of structural moieties that enhance the overall antioxidant activity.

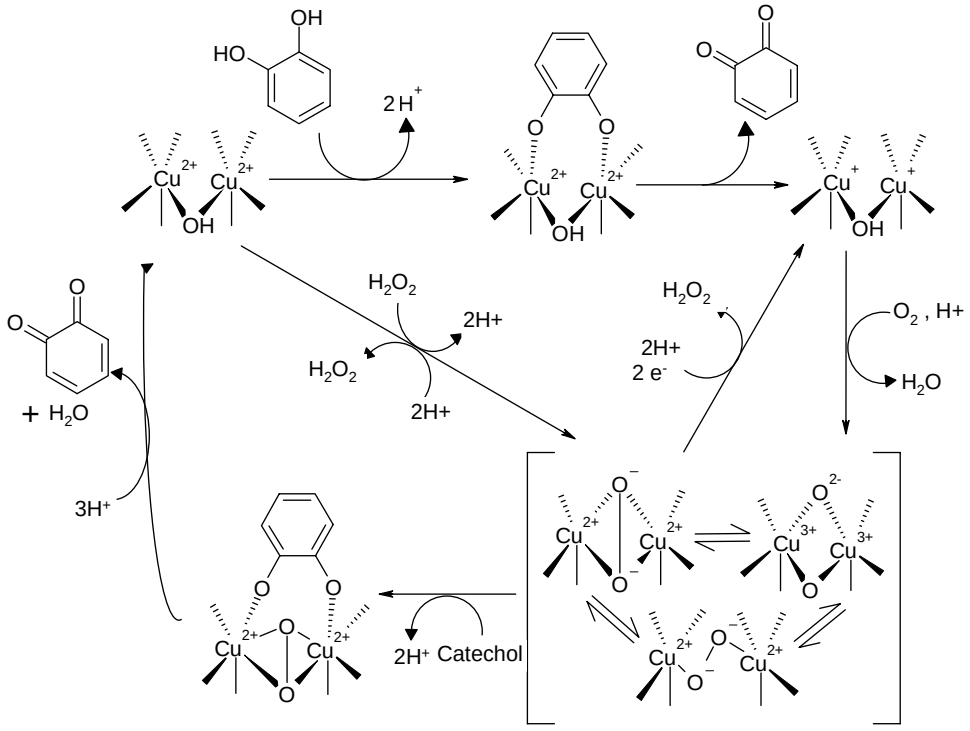

Figure (3-1) Purposed mechanism for polyphenol oxidation by Cu^{2+}-Aβ.[7]

Experimental

Chemicals and Materials for Metal Titrations and Kinetics Assays

The Aβ peptides (16 and 20 amino acid) were synthesized and purchased from the University of South Florida Peptide Center. The identity of the peptides ($DAEFR^{5}HDSGY^{10}EVHHQ^{15}KLVFF^{20}$ and $DAEFR^{5}HDSGY^{10}EVHHQ^{15}K$) were confirmed with a Bruker matrix-assisted laser desorption ionization time-of-flight (MALDI-TOF) mass spectrometer. The buffer used in all assays is 100 mM HEPES at pH 7.4 or 7.0, with small amount of chlex resin to demetalize the solution. EDTA was used in cleaning glass/plastic ware prior to usage, in order to prevent metal contamination. Deionized water of 18 MΩ was obtained from a Milli Q system (Millipore, Bedford, MA) and used for all cleaning and for preparation of stocks solutions. $CuSO_4$ and $CaCl_2$ were used for all experiments. All kinetic studies were run using a Varian CARY50 Bio-UV-Vis spectrophotometer.

Peptide Preparation

The molar absorptivity was determined by monitoring the absorbance of known concentrations of peptide dissolved in water at 280nm for the aromatic amino acids. Metal derivatives were prepared by the addition of a known concentration of metal to achieve a 1:1 metal to peptide ratio. Since Aβ tends to coagulate, fresh peptide stocks were prepared and used within 24 hours.

Dopamine and Flavonoid Oxidation assays

Using a constant Cu^{2+}-Aβ concentration (1-6μM) with a 1:1 Cu-to-peptide ratio, various substrate concentrations were assayed. The final volume of each assay is 1 mL at

pH 7.4 100mM HEPES and 298 K. The concentration of MBTH was kept in proportion with substrate concentration. Dopamine were varied from 0.1-2.5 mM and the MBTH-o-quinone product was monitored at 510 nm for 3-5 mins. Similar assays were constructed for epicatechin (EC), epigallocatechin gallate (EGCG), and epigallocatehin (EGC) and were monitored at their respective λ_{max} (460nm , 465nm, and 460 nm).

Hydrogen peroxide (H_2O_2) titration were performed with fixed catalyst and saturating conditions of substrate. The conditions were similar to non-H_2O_2 assays described above. H_2O_2 varied and the dopamine/EC/EGC/EGCG-MBTH product was monitored at their respective absorbencies. Additionally, experiments were preformed that varied substrate at a fixed catalyst and H_2O_2 concentration. These data were then fitted to the Hanes analysis to determine apparent and intrinsic dissociation constants.

Molar Absorptivity

The Molar Absorptivity (ε) was calculated by oxidizing a known concentration of substrate with tyrosinase with excess MBTH at the pH 7.4 100mM HEPES buffer. The ε for EGCG was found by the combination of value for EGC and gallic acid.

Substrates (pH 7.4)	Dopamine	EC	EGC	EGCG
ε (M-1 cm-1)	10095	10040	7159	7665
Wavelength (nm)	510	460	460	465

Table 3-1: Molar Absorptivity values for neurotransmitter and flavonoids

Inhibition Experiments

Conditions for inhibition experiments consisted of μM Cu^{2+}-Aβ, pH 7.4 or 7.0 HEPES 100 mM buffer, 293 K, and 1 ml total volume. The inhibitors used were

quercetin, fisetin, taxifolin, ascorbic acid, and pyridoxamine. For all inhibitors a Dixon plot was obtained by titrating inhibition into a fixed concentrations of dopamine, MBTH, and Cu^{2+}-Aβ. Then oxidation rates at different [dopamine] were determined in a fixed [I] and [Cu^{2+}-Aβ] to obtain the Lineweaver-Burk plots. Inhibition constants were determined from inhibition equations from Chapter 2.

Attenuation of inhibition was monitored by titrating Ca^{2+} into a fixed concentration of fisetin, dopamine, and Cu^{2+}-Aβ. Oxidation rate of dopamine was then determined at fixed concentration of fisetin, Cu^{2+}-Aβ, and $Ca^{2+}$to obtain kinetic parameters.

Results and Discussion

Green Tea

Dopamine is a catechol containing neurotransmitter found extensively throughout the body. Like other neurotransmitters, dopamine is used to amplify and regulate signals to dopamine receptors. An alteration in levels of dopamine (e.g. oxidation) is in general a hallmark of several neurodegenerative diseases.[7] Alzheimer's disease (AD) is associated with degradation of normal brain function which includes altered levels of neurotransmitters, influx of Ca^{2+}, and accumulation of protein fragments.[1,2] The results in figure 3-2 and 3-3 indicated Cu^{2+}-$A\beta^{1-16}$ and Cu^{2+}-$A\beta^{1-20}$ significantly accelerate aerobic oxidation of dopamine in terms of k_{cat} relative to auto-oxidation rate constant k_o = 1.59 x 10^{-8}. Furthermore, the additional 4 amino acids of Cu^{2+}-$A\beta^{1-20}$ seem to have a negligible effect on dopamine oxidation. Through metal ion reduction, reports have indicated the production of H_2O_2 by metallo-Aβ.[2] The results in figure (3-5) and (3-6) indicated that H_2O_2 significantly increases the rate of oxidation of dopamine. The oxidation rate dependent on H_2O_2 eventually plateaus, concluding H_2O_2 binds Cu^{2+}-Aβ and is turned over. Since both dopamine and H_2O_2 are considered substrates for Cu^{2+}-$A\beta^{1-16}$ and Cu^{2+}-$A\beta^{1-20}$, the data can be fitted to a bisubstrate random-binding equation to obtain both apparent and intrinsic dissociation constants K_{app} and $K_{m.}$ (Table 3-2).

The oxidation and generation of ROS in AD brains have suggested possible benefit from the consumption of foods with high antioxidant content.[9] A class of compounds reported to have antioxidant, antiradical, and influence on APP processing

are the green tea catechins (GTC).[10,11] The three GTCs were shown to be substrates for both Cu^{2+}-Aβ^{1-16} and Cu^{2+}-Aβ^{1-20} (Figures 3-2 – 3-4).

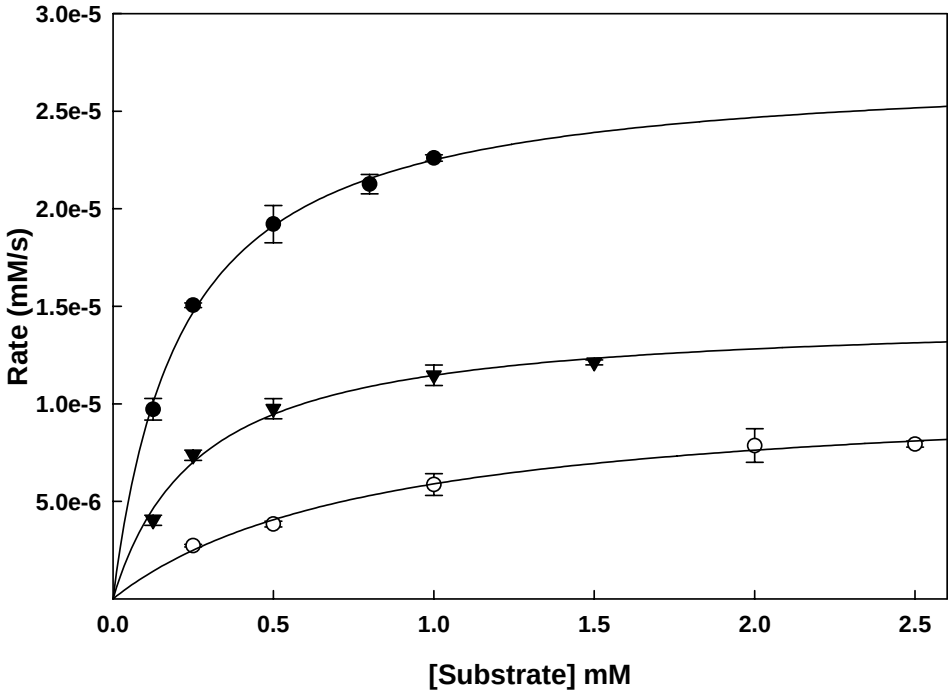

Cu^{2+}-Aβ^{16}	Dopamine	EC	EGCG
K_m (mM)	0.269 ± 0.033	0.830 ± 0.095	0.215 ± 0.012
V_{max} (mM/s)	(1.45 ± 0.06) x 10^{-5}	(1.08 ± 0.05) x10^{-5}	(2.73 ± 0.05) x 10^{-5}
k_{cat} (s^{-1})	4.83 x 10^{-3}	3.60x10^{-3}	9.10x10^{-3}
k_{cat} / K_m (mM^{-1} s^{-1})	0.0180	4.34x10^{-3}	.0423

Figure 3-2: Saturation kinetic profile for the oxidation of dopamine (▼), epicatechin (EC) (○), and epigallocatechin gallate (EGCG) (●) using Cu^{2+}-Aβ^{16} (3 μM) at 100 mM HEPES pH 7.4, 298K. Table includes kinetic parameters for dopamine, EC, and EGCG oxidation by Cu^{2+}-Aβ^{16}.

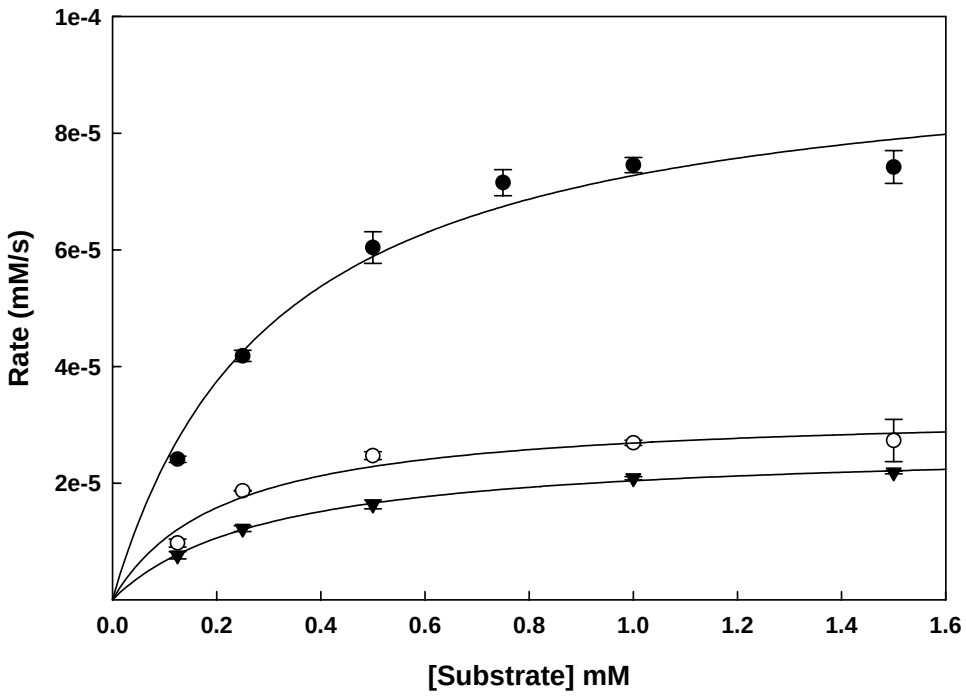

Cu^{2+}-$A\beta^{20}$	Dopamine	EC	EGCG
K_m (mM)	0.214 ± .050	0.302 ± 0.016	0.310 ± 0.053
V_{max} (mM/s)	(3.26 ± 0.22) x 10^{-5}	(2.66 ± 0.05) x10^{-5}	(9.52 ± 0.52) x 10^{-5}
k_{cat} (s^{-1})	4.66x10^{-3}	3.80x10^{-3}	.0136
k_{cat} / K_m (mM^{-1} s^{-1})	0.0218	0.0126	0.0439

Figure 3-3: Saturation kinetic profile for the oxidation of dopamine (○), epicatechin (EC) (▼), and epigallocatechin gallate (EGCG) (●) using Cu^{2+}-$A\beta^{20}$ (7 μM) at 100 mM HEPES pH 7.4 298K. Tables include kinetic parameters for dopamine, EC, and EGCG oxidation by Cu^{2+}-$A\beta^{20}$.

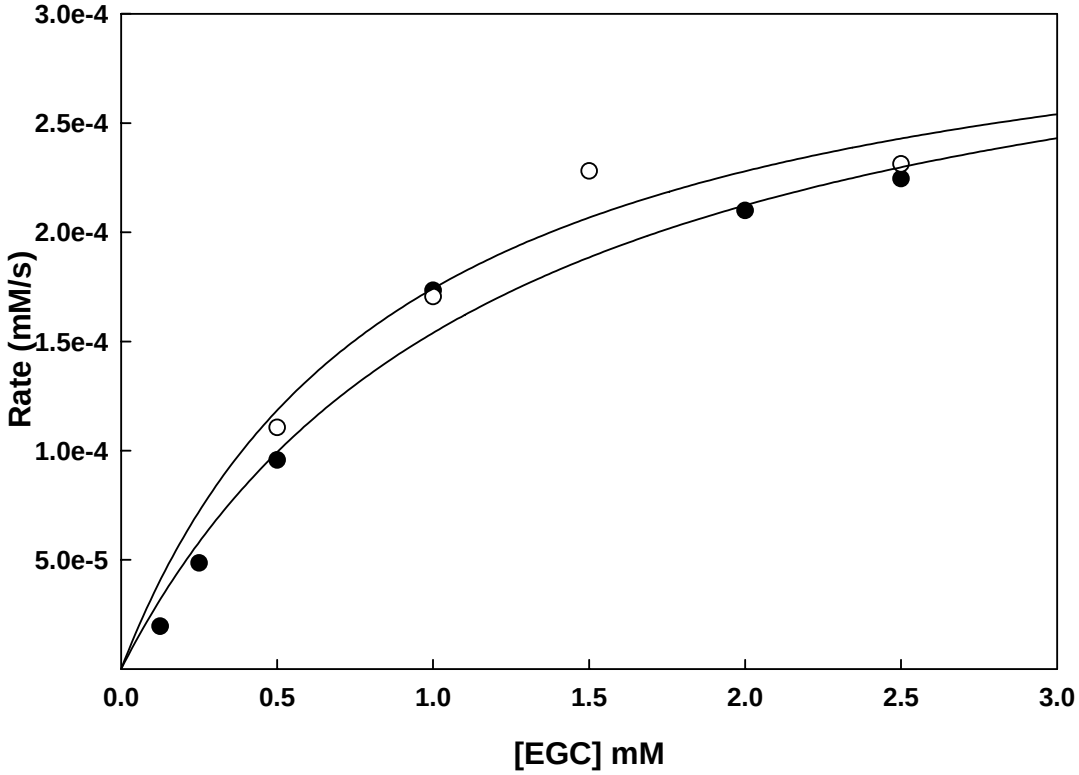

EGC	Cu^{2+}-Aβ^{16}	Cu^{2+}-Aβ^{20}
K_m (mM)	1.22 ± 0.28	8.91 ± 0.30
V_{max} (mM/s)	(3.42 ± 0.35) x 10^{-4}	(3.30 ± 0.43) x 10^{-4}
k_{cat} (s^{-1})	.114	.0825
k_{cat} / K_m (mM^{-1} s^{-1})	.0934	.00926

Figure 3-4: oxidation of epigallocatechin (EGC) by Cu^{2+}-Aβ^{20} (○)(4μM) and Cu^{2+}-Aβ^{16} (●)(3μM) at 100mM HEPES pH 7.4, 293 K. Table includes kinetic parameters for EGC oxidation by Cu^{2+}-A$\beta^{16,20}$.

Additionally, the effect of H_2O_2 on Cu^{2+}-Aβ catalysis was also monitored to obtain both apparent (K_{app}) and intrinsic (K_m) affinity constants. (Figure 3-5, 3-6 and Table 3-2). The K_{app}/K_m ratio can reveal details on the effect one substrate have on the affinity of other. Ratios above unity indicate one substrate decreases the affinity for the other, while those above unity indicate the opposite. For dopamine, EC, and EGCG, H_2O_2 seems to have little effect on the binding (close to unity). On the contrary, dopamine, EC, and EGCG seem to slightly increase the binding affinity for H_2O_2.

In addition to catechins, green tea is also an excellent source of ascorbic acid (AsA) and vitamin B_6 (B_6). Studies have shown both to serve as excellent antioxidants in addition to other vital roles in the human body. As shown in Figure (3-7,3-8), AsA is an excellent mixed type inhibitor for Cu^{2+}-$A\beta^{1-16}$ and Cu^{2+}-$A\beta^{1-20}$ toward dopamine oxidation. The most likely explanation is AsA may bind to the metal center and reduce Cu^{2+} to Cu^{+} thus preventing O2 from binding. Studies have shown AsA can increase the stability of GTCs, thus providing benefit by protecting antioxidants from premature oxidative breakdown. The other component in green tea is one of three derivates of vitamin B_6, pyridoxamine. Pyridoxamine is a critical component needed by the body, used by some enzymes for the production of neurotransmitters.[12] Furthermore, prydoxamine has been shown to inhibit ROS generated in the body.[12] As shown in figures (3-9, 3-10) pyridoxamine is a competitive inhibitor. The competitive inhibition pattern is most likely to be due to pyridoxamine weak affinity for Cu^{2+}.[12] This is further supported by the large K_i (in comparison to AsA).

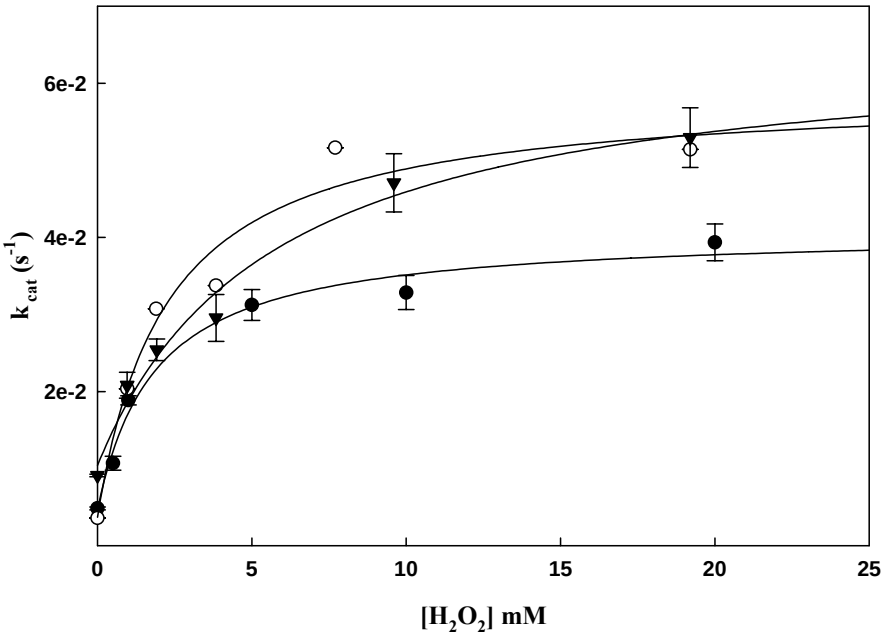

Figure 3-5: The effect of the concentration of H_2O_2 on the first-order rate constant kcat toward the Aβ 1-16 oxidation of Dopamine (●), Epicatechin (○), and epigallocatechin gallate (Δ).

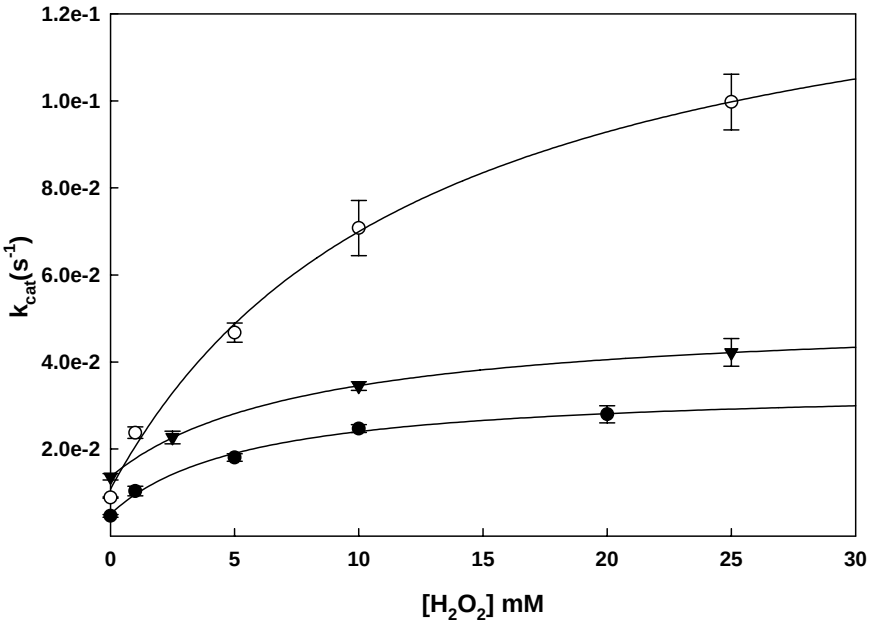

Figure 3-6: The effect of the concentration of H_2O_2 on the first-order rate constant kcat toward the Aβ 1-20 oxidation of Dopamine (●), Epicatechin (○), and epigallocatechin gallate (▼).

Substrate	Catalyst	K_{app}/K_m	$K_{app(H)} / K_{m(H)}$
Dopamine	Cu^{2+}-Aβ^{16}	.924	.228
Dopamine	Cu^{2+}-Aβ^{20}	1.39	1.18
EGCG	Cu^{2+}-Aβ^{16}	1.35	.771
EGCG	Cu^{2+}-Aβ^{20}	1.86	.924
EC	Cu^{2+}-Aβ^{16}	.554	.296
EC	Cu^{2+}-Aβ^{20}	1.43	.824

Table 3-2: Hanes analysis to compare the apparent (K_{app}) and intrinsic (K_m) affinity constants of H_2O_2 on substrate binding and vise versa.

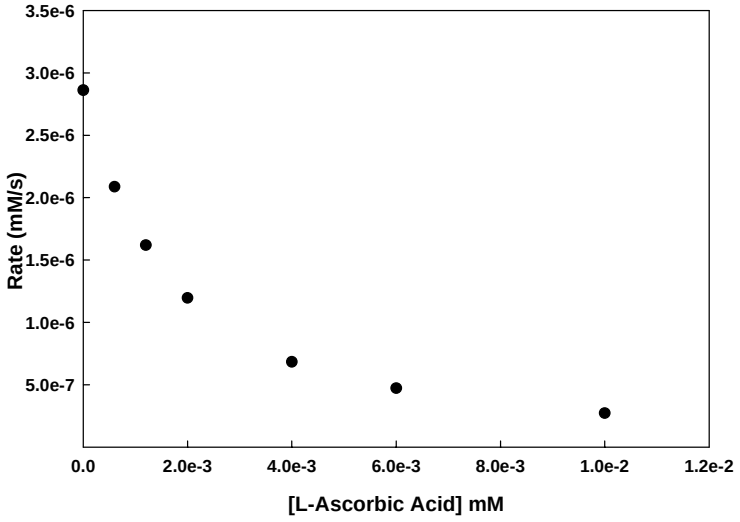

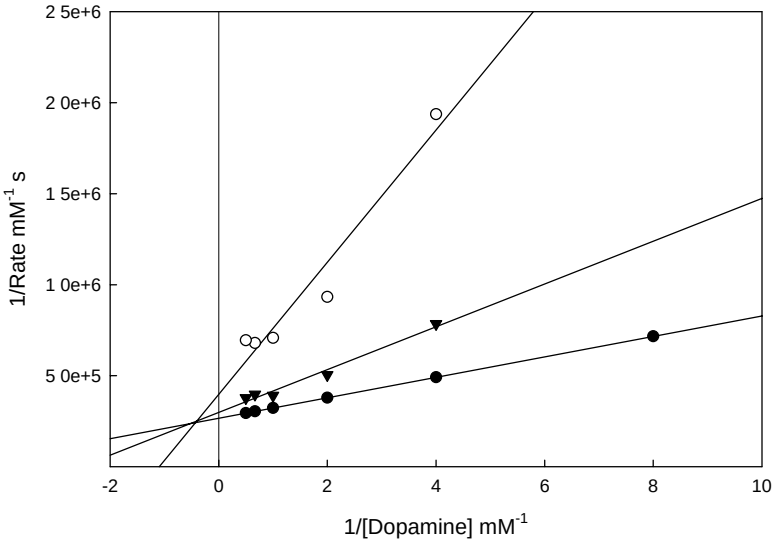

[Ascorbic Acid] mM $A\beta^{1-16}$	K_m (mM)	V_{max} (mM/s)
0.0	0.211 ± .053	(3.75 ± 0.24) x 10^{-6}
3.0 x 10^{-4}	0.372 ± .070	(3.25 ± 0.19) x 10^{-6}
1.2 x 10^{-3}	0.560 ± .178	(2.00 ± 0.23) x 10^{-6}
K_i= 1.37 µM		K_{is}= .302 µM

Figure 3-7: Inhibition of Cu^{2+}-$A\beta^{1-16}$ by ascorbic acid (AsA). (Top) AsA titration into fixed [Cu^{2+}-$A\beta^{1-16}$] , 1 mM Dopamine, 1 mM MBTH. (Bottom) Titrating dopamine at fixed concentrations of AsA. Table includes effect of [AsA] on kinetic parameters including inhibition constants for mixed-type inhibition. Assays done at pH 7.4 100mM HEPES buffer , 293K.

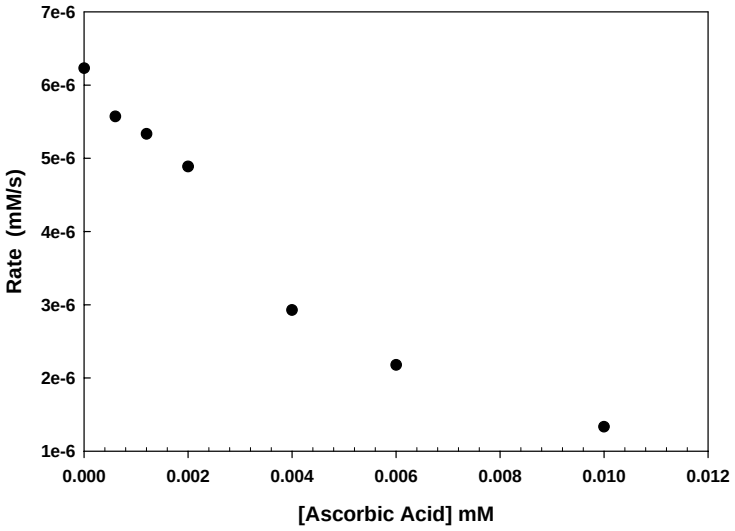

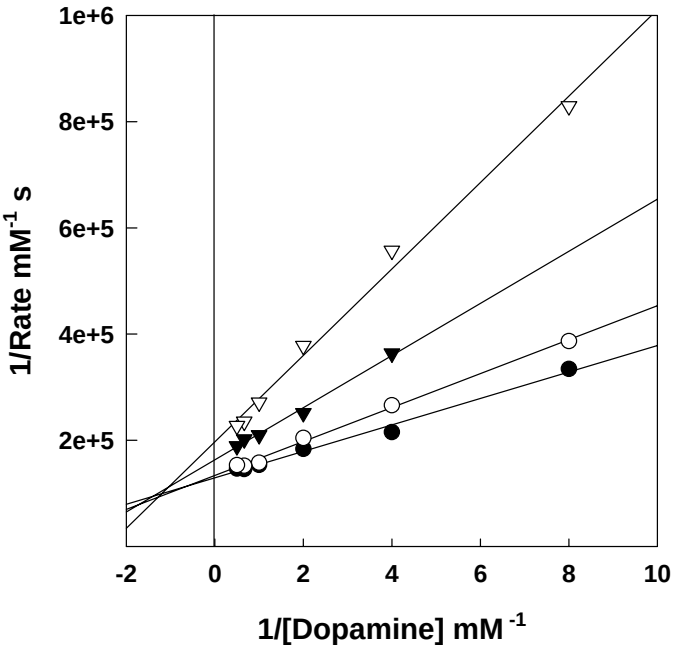

[Ascorbic Acid] mM $A\beta^{1-20}$	K_m (mM)	V_{max} (mM/s)
0.0	0.177 ± .016	(7.57 ± 0.16) x10^{-6}
5.0 x 10^{-4}	0.248 ± .026	(7.58 ± 0.21) x 10^{-6}
2.0 x 10^{-3}	0.237 ± .029	(5.84 ± 0.19) x 10^{-6}
3.0 x 10^{-3}	0.523 ±.044	(5.61 ± 0.17) x10^{-6}
K_i = 8.59 μM		K_{is} = 1.00 μM

Figure 3-8: Inhibition of Cu^{2+}-$A\beta^{1-20}$ by ascorbic acid (AsA). (Top) AsA titration into fixed Cu^{2+}-$A\beta^{1-20}$, 1mM Dopamie, 1mM MBTH. (Bottom) Titrating dopamine at fixed concentrations of AsA. Table includes effect of [AsA] on kinetic parameters. including inhibition constants for mixed type inhibition. Assays done at pH 7.4 100mM HEPES buffer , 293K.

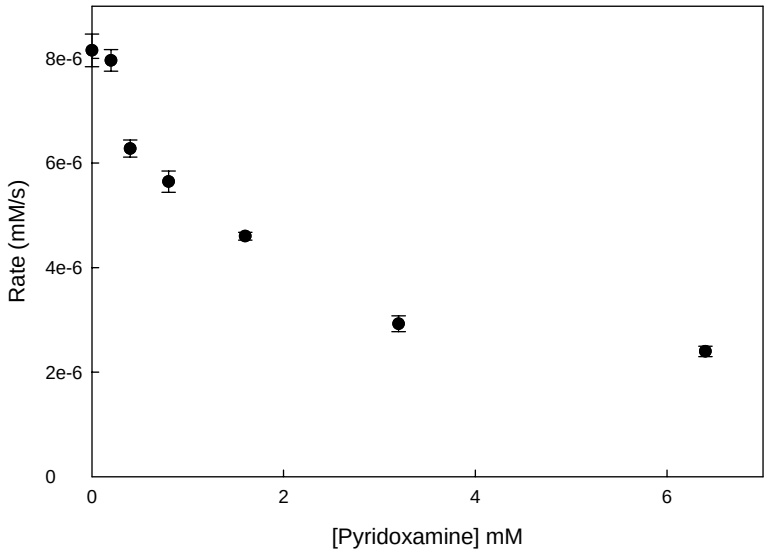

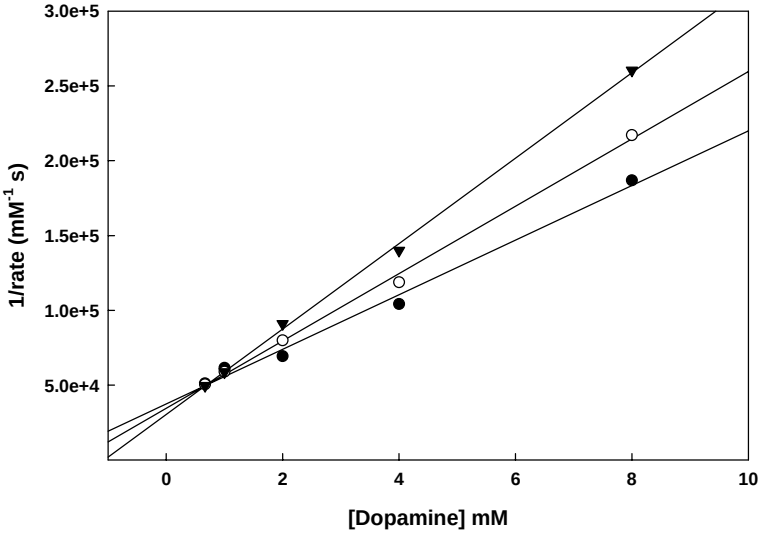

[Pyridoxamine] mM $A\beta_{20}^{1-}$	K_m (mM)	V_{max} (mM/s)
0.0 (●)	0.381 ± 0.063	(2.39 ± 0.14) x10^{-5}
0.5 (○)	0.590 ± 0.031	(2.74 ± 0.61) x10^{-5}
1.0 (▼)	0.959 ± 0.061	(3.31 ± 0.11) x10^{-5}
K_i= .911 mM		

Figure 3-9: Inhibition of Cu^{2+}-$A\beta^{1-20}$ by Pyridoxamine (B_6). (Top) B_6 titration into fixed [Cu^{2+}-$A\beta^{1-20}$], 1 mM Dopamie, 1mM MBTH. (Bottom) Titrating dopamine at fixed concentrations of B_6. Table includes effect of [B_6] on kinetic parameters, including inhibition constants for competitive inhibition. Assays done at pH 7.4, 100mM HEPES buffer , 293K.

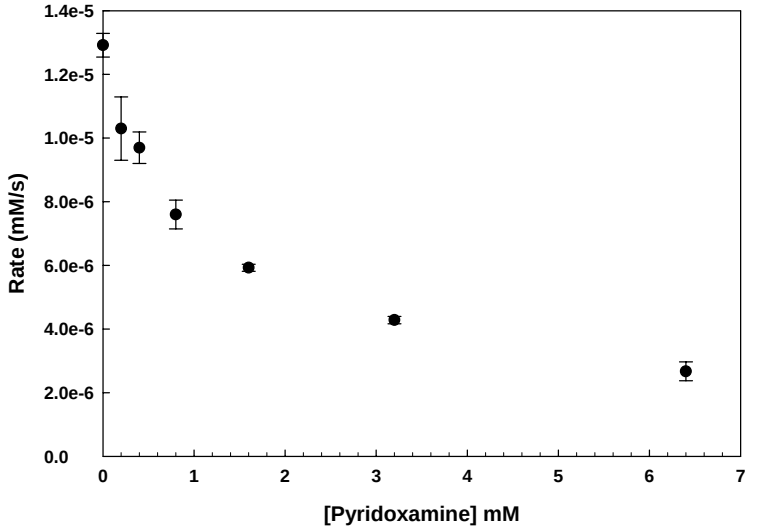

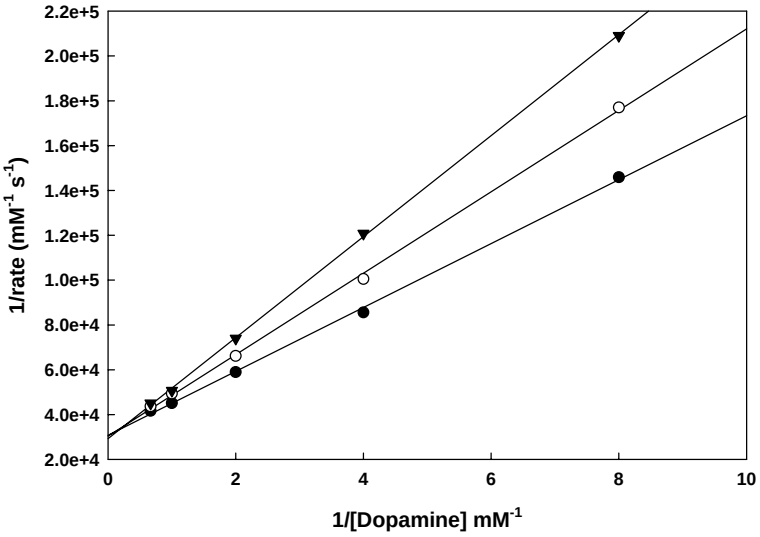

[Pyridoxamine] mM $A\beta^{1-16}$	K_m (mM)	V_{max} (mM/s)
0.0 (●)	0.419 ± 0.020	(3.11 ± 0.05) x 10^{-5}
0.4 (○)	0.541 ± 0.015	(3.13 ± 0.04) x 10^{-5}
0.8 (▼)	0.746 ± 0.052	(3.37 ± 0.11) x 10^{-5}
K_i= 1.03 mM		

Figure 3-10: Inhibition of Cu^{2+}-$A\beta^{1-16}$ by Pyridoxamine (B_6). (Top) B_6 titration into fixed Cu^{2+}-$A\beta^{1-16}$, 1mM Dopamie, 1mM MBTH. (Bottom) Titrating dopamine at fixed concentrations of B_6. Table includes effect of [B_6] on kinetic parameters. including inhibition constants for competitive inhibition. Assays done at pH 7.4 100mM HEPES buffer, 293K.

Quercetin, Fisetin, and Taxifolin

There are over 6000 flavonoids which differ in both structure and bioactivity.[13,14] Studies have been done concerning the "best" structure for the binding of redox-active metal in addition to antioxidant and antiradical activity.[13,14] The flavonoids used in this study are structurally similar, differing only by the absence and presence of the enolate or β-keto-phenolate. The results show quercetin, fisetin, and taxifolin to be competitive inhibitiors of Cu^{2+}-Aβ oxidation of dopamine. Quercetin contains both the presence of the enolate or β-keto-phenolate and shows to be an excellent competitive inhibitor, yielding a K_i (4 μM) almost equivalent to the [Cu^{2+}-Aβ] (Figure 3-11). Fisetin does not contain the β-keto-phenolate, but it is near equivelant to querctin in terms of K_i. (Figure 3-12, 3-13). Taxifolin contains the β-keto-phenolate but is missing the double bond on the enolate. Taxifolin shows also to be a competitive inhibitor with a K_i 100 times higher then quercetin or fisetin. (Figure 3-15, 3-16) The results, in combination with the fact that catechins are substrates, reveal that the 3-hydroxy on the C-ring is required for inhibition. Furthermore the presence of the enolate allows for a better affinity for Cu^{2+}. To further distinguish between the β-keto-phenolate and enolate, fisetin was used in conjunction with Ca^{2+}. The Ca^{2+} titration in figure (3-14) reveal that Ca^{2+} attenuate the inhibition of fisetin oxidation of dopamine by Cu^{2+}-Aβ[16]. This result concludes that Ca^{2+} is binding in the same place as Cu^{2+} the enolate.

The general mechanism for AD is believed to involve metal-centers ROS. This study proposes the use of green tea components as suicide substrates and antioxidants for a possible way to slow the oxidation of neurotransmitters. In addition, citrus flavonoids quecetin, fisetin, taxifolin have shown to be excellent inhibitors of both Cu^{2+}-Aβ[16] and

Cu^{2+}-$A\beta^{20}$. The Ca^{2+} binding properties allude to certain flavonoids to serve as Ca^{2+} "sponge", potentially reducing the influx of Ca^{2+} seen in AD. The activity and inhibition of both the Cu^{2+}-$A\beta^{16}$ and Cu^{2+}-$A\beta^{20}$ conclude that the 4 amino acid differences make no significant contribution to activity.

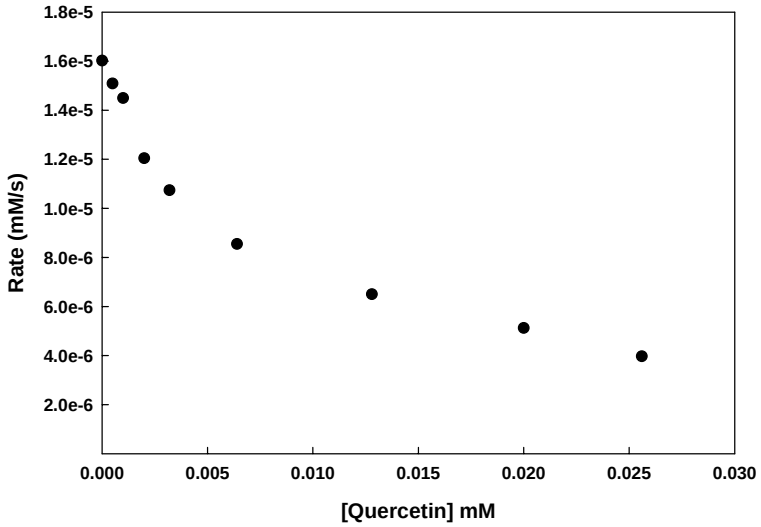

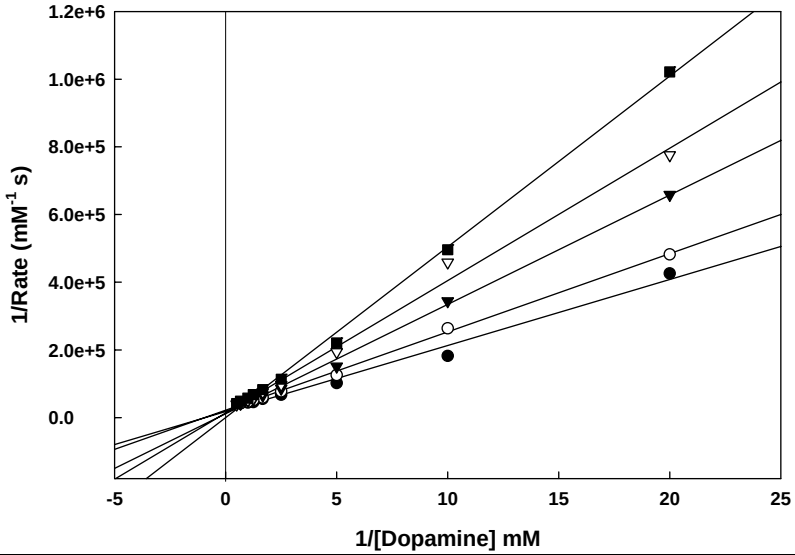

[Quercetin] mM $A\beta^{16}$	K_m (mM)	V_{max} (mM/s)
0	0.467 ± 0.053	(3.26 ±0.15) x 10^{-5}
2.0 x 10^{-3}	0.699 ± 0.052	(3.59 ± 0.13) x10^{-5}
4.0 x 10^{-3}	0.962 ± 0.082	(3.92 ± 0.18) x 10^{-5}
6.0 x 10^{-3}	1.31 ± 0.16	(4.39 ± 0.29) x 10^{-5}
8.0 x 10^{-3}	1.57 ± 0.12	(4.32 ± 0.19) x 10^{-5}
K_i= .004 mM		

Figure 3-11: Quercetin inhibition of Cu^{2+}-$A\beta^{1-16}$ oxidation of dopamine. (Top) Quercetin titration into fixed [Cu^{2+}-$A\beta^{1-16}$], [Dopamine]. [MBTH]. (Bottom) Titrating dopamine at fixed concentrations of quercetin. Table includes effect of [Quercetin] on kinetic parameters including inhibition constants for competitive inhibition. Assays done at pH 7.0 100mM HEPES buffer , 293K. (●), .002(○), .004 (▼), .006(Δ), .008mM (■) of inhibitor**.**

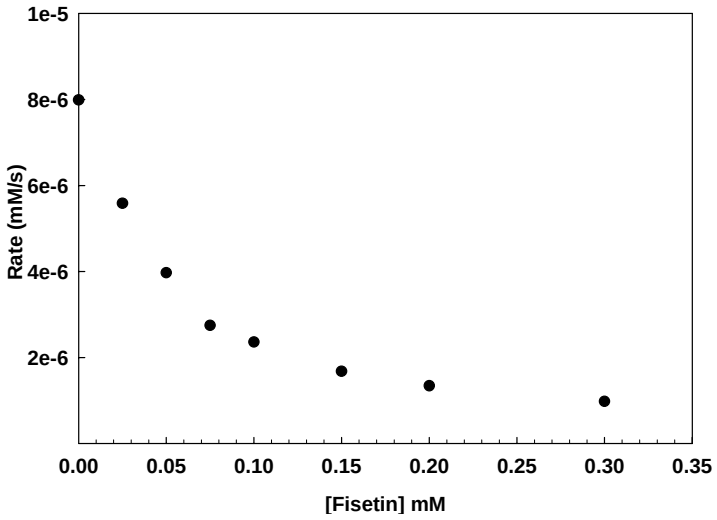

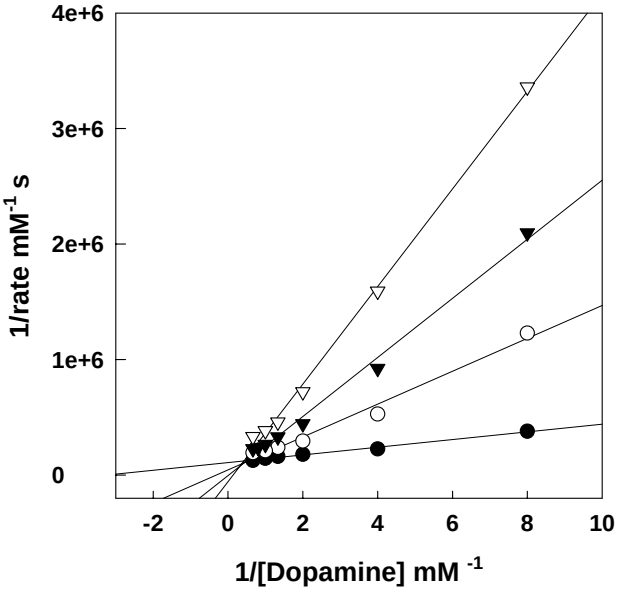

[Fisetin] mM $A\beta^{1-20}$	K_m (mM)	V_{max} (mM/s)
0	0.307 ± 0.039	(9.22 ± 0.37) x10^{-6}
1.25 x 10^{-2}	0.756 ± 0.148	(8.12 ± 0.75) x10^{-6}
2.50 x 10^{-2}	1.73 ± 0.35	(9.83 ± 0.13) x 10^{-6}
5.00 x 10^{-2}	2.03 ± 0.78	(7.40 ± 0.19) x10^{-6}
K_i= .009 mM		

Figure 3-12: Fisetin inhibition of Cu^{2+}-$A\beta^{1-20}$ oxidation of dopamine. (Top) Fisetin titration into fixed [Cu^{2+}-$A\beta^{1-16}$], [Dopamine]. [MBTH]. (Bottom) Titrating dopamine at fixed concentrations of fisetin. Table includes effect of [fisetin] on kinetic parameters including inhibition constants for competitive inhibition. Assays done at pH 7.4, 0 mM (●), .0125(○), .025 (▼), .05(Δ), of inhibitor.

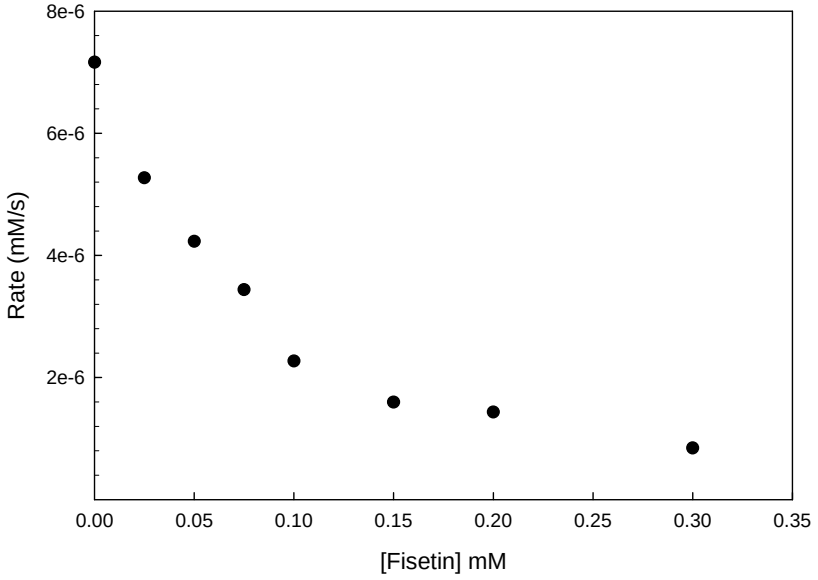

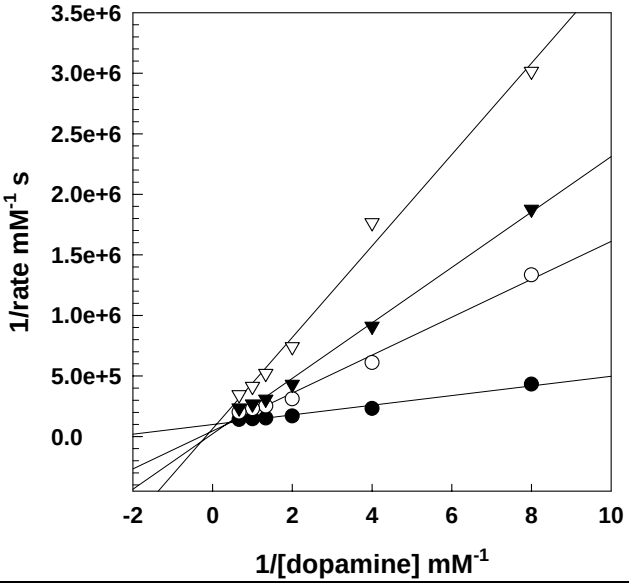

[Fisetin] mM $A\beta^{1-16}$	K_m (mM)	V_{max} (mM/s)
0.00	0.271 ± 0.040	(8.71 ± 0.39) x 10^{-6}
1.25 x 10^{-2}	0.830 ± 0.176	(7.97 ± 0.83) x 10^{-6}
2.50 x 10^{-2}	1.31 ± 0.34	(8.31 ± 1.24) x 10^{-6}
5.00 x 10^{-2}	2.32 ± 0.69	(7.59 ± 1.55) x10^{-6}
K_i= .007 mM		

Figure3-13: Fisetin inhibition of Cu^{2+}-$A\beta^{1-16}$ oxidation of dopamine. (Top) Fistein titration into fixed [Cu^{2+}-$A\beta^{1-16}$], [Dopamine]. [MBTH]. (Bottom) Titrating dopamine at fixed concentrations of fistein. Table includes effect of [fistein] on kinetic parameters including inhibition constants for competitive inhibition. Assays done at pH 7.4, 0 mM (●), .0125(○), .025 (▼), .05(Δ),of inhibitor.

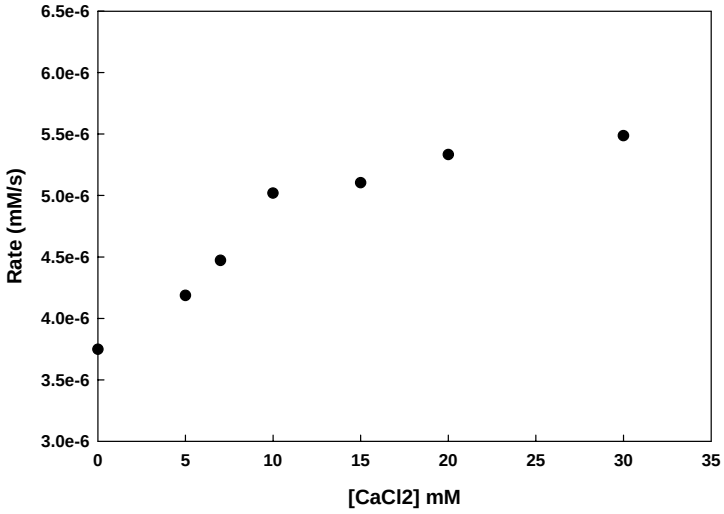

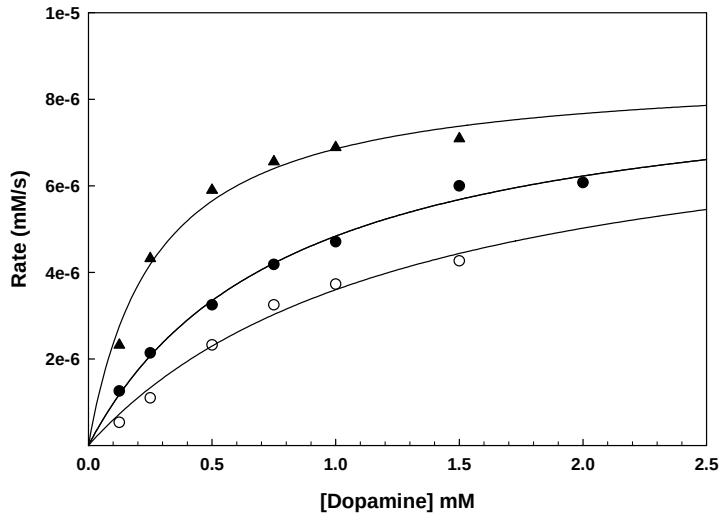

Fisetin - Ca^{2+} $A\beta^{1-16}$	Fistein 0 mM	Fistein .025 mM	Fistein .025 mM Ca^{2+}
K_m (mM)	0.271 ± 0.040	1.310 ± 0.337	0.806 ± 0.088
V_{max} (mM/s)	(8.71 ± 0.39) x 10^{-6}	(8.32 ± 1.24) x 10^{-6}	(8.73 ± 0.41) x 10^{-6}
k_{cat} s^{-1}	0.003	0.003	0.003
k_{cat}/K_m (mM^{-1} s^{-1})	0.011	0.002	0.004

Figure 3-14: Ca^{2+} effect on Fistein inhibition of Cu^{2+}-$A\beta^{1-16}$ oxidation of dopamine. (Top) Ca^{2+} titration in fixed [Cu^{2+}-$A\beta^{1-16}$], [Dopamine], and [Fisetin]. (Bottom) Dopamine titrations without fisetin (▲), with fisetin (○), and with fisetin + Ca^{2+} ([Ca^{2+}] = 30 mM)(●). Table includes kinetic parameters.

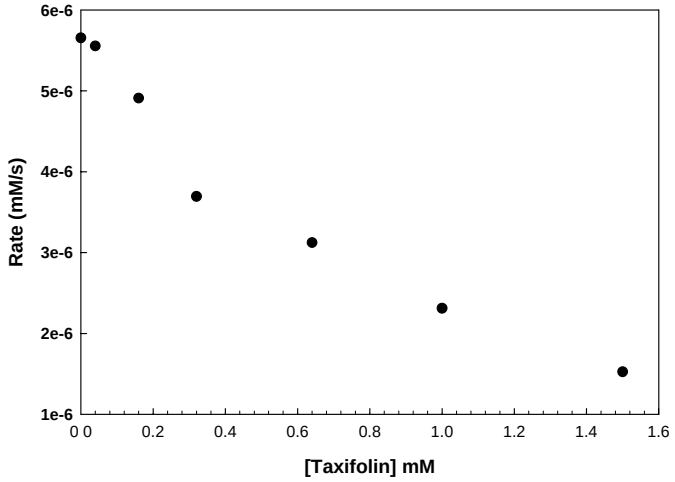

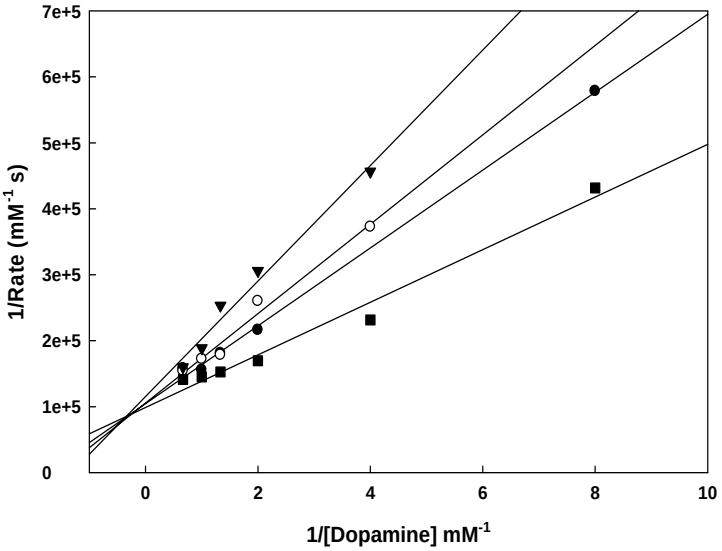

[Taxifolin] mM $A\beta^{1-16}$	K_m (mM)	V_{max} (mM/s)
0.00	0.271 ± 0.040	(8.71 ± 0.39) x 10^{-6}
0.16	0.392 ± 0.075	(8.38 ± 0.57) x 10^{-6}
0.32	0.670 ± 0.149	(9.66 ± 0.97) x 10^{-6}
0.64	1.23 ± 0.282	(1.14 ± 0.15) x10^{-5}
K_i = 0.216 mM		

Figure3-15: Taxifolin inhibition of Cu^{2+}-$A\beta^{1-16}$ oxidation of dopamine. (Top) Taxifolin titration into fixed [Cu^{2+}-$A\beta^{1-16}$], [Dopamine]. [MBTH]. (Bottom) Titrating dopamine at fixed concentrations of taxifolin. Table includes effect of [Taxifolin] on kinetic parameters including inhibition constants for competitive inhibition. Assays done at pH 7.4, 0 (■), .16 (●), .32 (○), .64 mM(▼),of inhibitor.

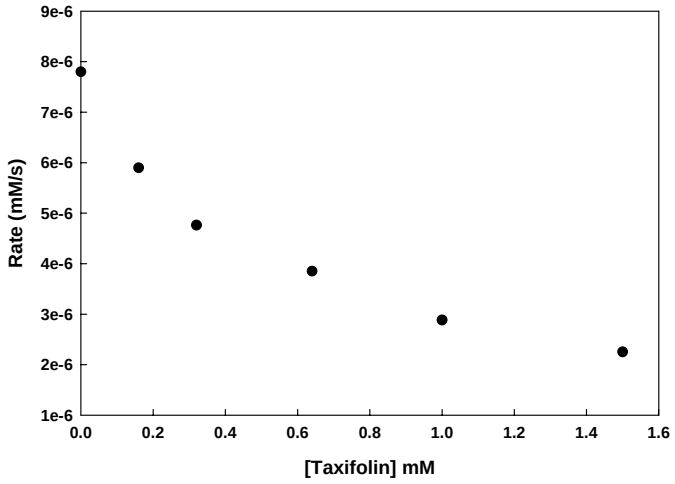

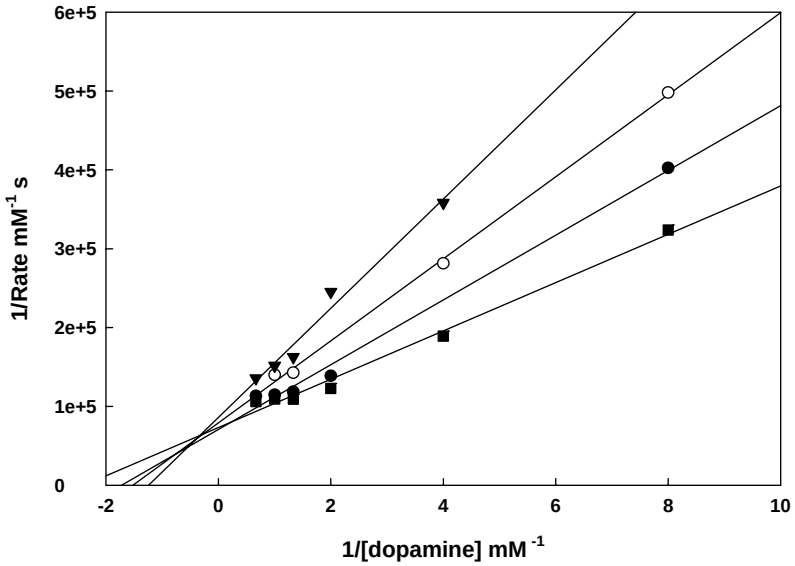

[Taxifolin] mM $A\beta^{1-20}$	K_m (mM)	V_{max} (mM/s)
0.00	0.290 ± .0585	(1.19 ± 0.08) x 10^{-5}
0.16	0.331 ± .0663	(1.15 ± 0.08) x 10^{-5}
0.32	0.539 ± .102	(1.10 ± 0.09) x 10^{-5}
0.64	0.729 ± .150	(1.12 ± 0.11) x 10^{-5}
K_i= 0.372 mM		

Figure3-16: Taxifolin inhibition of Cu^{2+}-$A\beta^{1-20}$ oxidation of dopamine. (Top) Taxifolin titration into fixed [Cu^{2+}-$A\beta^{1-20}$], [Dopamine]. [MBTH]. (Bottom) Titrating dopamine at fixed concentrations of taxifolin. Table includes effect of [Taxifolin] on kinetic parameters including inhibition constants for competitive inhibition. Assays done at pH 7.4, 0 (■), .16 (●), .32 (○), .64 mM(▼),of inhibitor.

Closing Remarks

With plaques composed of Aβ in addition to redox active metal, the results indicate their combination can result in oxidative damage. As shown, different forms of metallo-Aβ can oxidative neurotransmitters which may be a cause or effect of AD. This thesis focuses on the possible use of natural antioxidants to slow or inhibit this oxidative damage. Flavonoids have been studied extensively and are considered to provide therapeutic effect for numerous diseases. Here, the GTCs were shown to be oxidized and can potentially serve as suicide substrates. In addition vitamins AsA and B_6 were shown to inhibit the metallo-Aβ redox chemistry, possibly by reducing or chelating the metal. This study extents into the debate over the "best" flavonoid, by examining the properties of several common moieties. The GTCs, quercetin, fisetin, and taxifolin all vary specific functional groups and through inhibition of metallo-Aβ can determine thoughts of most benefit. The results indicate that the enolate is the most important in terms of metal chelation. The absence of the β-keto-phenolate seems to have no effect on the inhibition, while the opposite it true for the 2-3 alkene.

Reference

1) Gaggelli, E,. Kozlowski, H,. Valensin, D,. and Valensin G. (2006) Copper homeostasis and neurodegenerative disorders (Alzheimer's, prion, and Parkinson's diseases and amyotrophic lateral sclerosis). Chem. Rev., 106, 1994-2044.

2) Huang, X., Atwood, S, C., Hartshorn, A, M., Multhaup, G., Goldstein, E, L., Scarpa, C, R., Cuajungco. P, M., Gray, N, D., Lim, J., Moir, D, R., Tanzi, E, R. and Bush, I, A. (1999) The Aβ Peptide of Alzheimer's Disease Directly Produces Hydrogen Peroxide through Metal Ion Reduction. *Biochemistry,* 38, 7609 -7616

3) Xie, C, W. (2004) Calcium-regulated signaling pathways: role in amyloid beta-induced synaptic dysfunction. Neuromolecular Med., 6, 53-64.

4) Huang, X., Moir, D, R., Tanzi, E, R., Bush, I., A., and Rogers, T, R. (2004) Redox-Active Metals, Oxidative Stress, and Alzheimer's Disease Pathology. Ann. N.Y. Acad. Sci. 1012, 153–163.

5) Mekmouche, Y., Coppel, Y., Hochgrafe, K., Guilloreau, L., Talmard, C., Mazarguil, H. and Faller, P. (2005) Characterization of the ZnII binding to the peptide amyloid-beta1-16 linked to Alzheimer's disease. Chembiochem., 6, 1663-71.

6) Gnanakaran, S., Nussinov, R. and Garcia, A. E. (2006) Atomic-Level Description of Amyloid β-Dimer Formation. J. Am. Chem. Soc. 128, 2158-2159.

7) Da Silva, GFZ., Tay, WM., and Ming, L. (2005) Catechol Oxidase-like Oxidation Chemistry of the 1–20 and 1–16 Fragments of Alzheimer's Disease-related β-Amyloid Peptide J. Bio. Chem., 280, 16601-16609.

8) Mattson, M. (2000) Apoptosis in Neurodegenerative Disorders. Mol. Cell. Bio., 1, 120-129.

9) Casetta, I., Govni, V., and Granieri E. (2005) Oxidative stress, antioxidants and neurodegenerative diseases. Curr. Pharm. Des., 11, 2033-52.

10) Choi, Y, T., Jung, C, H., Lee, S, R., Bae, J, H., Baek, W, K., Suh, M, H., Park, J., Park, C, W. and Suh, S, I. (2001) The green tea polyphenol (-)-epigallocatechin gallate attenuates beta-amyloid-induced neurotoxicity in cultured hippocampal neurons. Life Sci. 70, 603-614.

11) Weinreb, O., Mandel, S., Amit, T., and Youdim, M. (2004) Neurological mechanisms of green tea polyphenols in Alzheimer's and Parkinson's diseases. J. of Nutrition. Biochem. 15, 506-516.

12) Voziyan, A, P. and Hudson, G, B. (2005) Pyridoxamine: The Many Virtues of a Maillard Reaction Inhibitor. Ann. N.Y. Acad. Sci., 1043, 807–816.

13) Matsuda, H., Wang, T., Managi, H. and Yoshikawa, M. (2003) Structural requirements of flavonoids for inhibition of protein glycation and radical scavenging activities. Bioorganic and Medicinal Chem., 11, 5317-5323.

14) Thompson, M. and Williams, C. R. (1976) Antioxidant Potential of Ecklonia cavaon Reactive Oxygen Species Scavenging, Metal Chelating, Reducing Power and Lipid Peroxidation Inhibition. Analytica Chimica Acta, 85, 375-381.